

Nanotribology: nonlinear mechanisms of friction

N. Manini, O.M. Braun, and A. Vanossi

Abstract Friction with its related nonlinear dynamics is a vast interdisciplinary field, involving complex physical processes over a wide range of length and time scales. The accelerated progress in experimental and computational techniques, often leading to complex detailed dynamical patterns, has vigorously stimulated the search and implementation of idealized experimental frameworks and simpler mathematical models, capable of describing and interpreting, in a more immediate way, the essential physics involved in nonlinear sliding phenomena.

1 Introduction

Frictional motion plays a central role in diverse systems and phenomena that span vast ranges of scales, from the nanometer contacts inherent in micro- and nanomachines [1] and biological molecular motors [2] to the geophysical scales characteristic of earthquakes [3]. Due to its enormous practical importance, the problem has stimulated progress over the centuries. Historical figures from Leonardo da Vinci onwards have brought friction into the field of physics, with the formulation of time-honored phenomenological frictional laws, which have been referred to as the Coulomb-Amontons laws. These statements can be summarized as follows: (*i*) fric-

N. Manini

Dipartimento di Fisica, Università degli Studi di Milano, Via Celoria 16, 20133 Milano, Italy, e-mail: nicola.manini@mi.infm.it

O.M. Braun

Institute of Physics, National Academy of Sciences of Ukraine, 46 Science Avenue, Kiev 03028, Ukraine, e-mail: obraun.gm@gmail.com

A. Vanossi

CNR-IOM Democritos National Simulation Center, Via Bonomea 265, 34136 Trieste, Italy and International School for Advanced Studies (SISSA), Via Bonomea 265, 34136 Trieste, Italy, e-mail: vanossi@sissa.it

tional force is independent of the apparent area of contact; *(ii)* frictional force is proportional to the normal load; *(iii)* kinetic friction (the force to keep relative motion at constant speed) does not depend on the sliding velocity and is smaller than static friction (the force needed to initiate motion between two contacting bodies at rest). Serious attempts were made in the first half of the 20th century toward a microscopic understanding of these laws [4]. Whereas the basic physics underlying sliding friction — non equilibrium statistical mechanics of solids, sheared fluids, and moving surfaces — is in principle quite exciting, the field as a whole has (even if with notable exceptions) failed to attract adequate interest by the physicist until the last few decades, mainly because of a lack of microscopic experimental data.

Three quiet revolutions, of broad nature and unrelated to friction, are radically changing this state of affairs. First, progress in the general area of complexity provided new tools to tackle non-equilibrium disordered systems with interacting degrees of freedom. Second, and crucial, the developments in nanotechnology extended the study of friction and permitted its analysis on well-characterized materials and surfaces at the nano and microscale [5]. Notably the invention of scanning tip instruments of the Atomic Force Microscope (AFM) family [6] has opened *nanofriction* as a brand new avenue, the use of the Surface Force Apparatus (SFA) [7] has led to the systematic studies of confined mesoscopic systems under shear, and the Quartz Crystal Microbalance (QCM) [8,9] has allowed us to measure the inertial sliding friction of adsorbate submonolayers. Thanks to these methods, a mass of fresh data and information on well defined systems has accumulated in the last two decades. Third, computer simulations have had a strong boost, also allowed by the fantastic growth of computer power. The numerical study of frictional models on one hand, and direct atomistic molecular dynamics (MD) simulations on the other hand, are jointly advancing our theoretical understanding [10]. Invaluable initial reviews of the progress in our understanding of sliding friction can be found in the books [11] and [12].

Despite the importance of friction and the growing efforts in the field, many key aspects of friction dynamics are not yet fully understood. Fundamental theory is still difficult in all fields of sliding friction, including nanofriction, since the sliding motion generally involves sudden nonlinear stick-slip events, that cannot be treated within traditional theoretical approaches such as linear-response theory and hydrodynamics. Experiments in tribology have long suffered from the inability to directly observe what takes place at the sliding interface. Although AFM, SFA and QCM techniques have identified many friction phenomena on the nanoscale, many interpretative pitfalls still result from indirect or ex-situ characterization of contact surfaces. In the present chapter, we will briefly cover some aspects, progress, and problems in the current modeling and simulation of sliding friction, from nano to mesoscale.

One of the main difficulties in understanding and predicting frictional response is the intrinsic complexity of highly nonlinear and non-equilibrium processes going on in any tribological contact, which include detachment and reattachment of multiple microscopic junctions (bonds) between the surfaces in relative motion while still in contact [1,2,13]. Therefore friction is intimately related to instabilities that occur on

a local microscopic scale, inducing an occasional fast motion of the corresponding degrees of freedom even if the slider's center-of-mass velocity is extremely small. Understanding the physical nature of these instabilities is crucial for the elucidation of the mechanism of friction, as we will emphasize below.

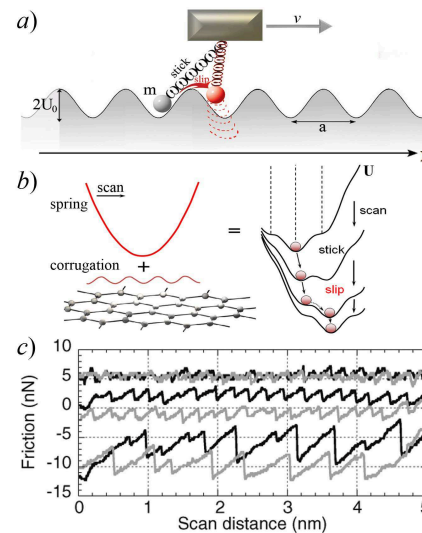
The present chapter covers the following different types of theoretical approach to sliding friction: “minimalistic” models (MMs) described in Secs. 2 and 3, atomistic MD simulations considered in Sec. 4, and mesoscopic earthquakelike (multicontact) models briefly discussed in Sec. 5 (phenomenological rate-state models will not be considered here; this topic is covered, e.g., in [14]).

2 The Prandl-Tomlinson Model

The Prandtl-Tomlinson (PT) model [16, 17] is the most successful and influential MM so far suggested for description of nanoscale friction. In particular, it addresses friction force microscopy (FFM) where friction forces are measured by dragging an AFM tip along a surface. Qualitative conclusions drawn with this model provide guidance to understand friction at the nanoscale, that often retain their validity in more advanced models and MD simulations.

PT assumes that a point-like mass m (e.g., mimicking the AFM tip) is dragged over a one-dimensional (1D) sinusoidal potential representing the interaction between the tip and a crystalline substrate. The point-like tip is pulled by a spring of effective elastic constant K , extending between the tip position x and the position of the microscope support stage, that is driven with a constant velocity v relative to the substrate, see Fig. 1a. Thus, the total potential experienced by the tip consists of two

Fig. 1 (a) The Prandl-Tomlinson model; (b) Energy landscape for a soft spring (low K). The total potential (harmonic spring + sinusoidal substrate) exhibits different metastable minima, giving rise to the stick-slip behavior. (c) A representative experimental friction pattern, for increasing load. Lateral AFM force vs position traces demonstrate transitions from smooth sliding (top) to single (middle) and mostly double slips (bottom). (Reproduced from [15]). Similar patterns can be generated within the PT model.



parts, the tip-substrate interaction and the elastic interaction between the tip and the support, and can be written as

$$U(x, t) = U_0 \cos\left(\frac{2\pi}{a}x\right) + \frac{K}{2}(x - vt)^2, \quad (1)$$

where $2U_0$ is the amplitude and a is the period of the tip-substrate potential. Note that in an AFM experiment the actual ‘‘spring constant’’ mimicked by K in the PT model is not only due to the torsional stiffness of the cantilever but includes also the contribution from the lateral stiffness of the contact. There is no attempt in the model to describe realistically the energy dissipation into the substrate — all dissipation is described by a viscous force $-m\gamma\dot{x}$, where γ is a damping coefficient. The instantaneous lateral friction force measured in FFM experiments reads $F = -K(x - vt)$, and the kinetic friction F_k is the time average of F .

The PT model predicts two different modes for the tip motion, depending on the dimensionless parameter $\eta = 4\pi^2 U_0 / (Ka^2)$, which represents the ratio between the stiffness of the tip-substrate potential and that of the pulling spring. When $\eta < 1$, the total potential $U(x)$ exhibits only one minimum and the time-dependent sliding motion is smooth; for $\eta > 1$ two or more minima appear in $U(x)$, and the sliding is discontinuous, characterized by stick-slip, Fig. 1b. The value $\eta = 1$ represents the transition from smooth sliding to slips by one lattice site (single-slip regime).

Physically, stick-slip motion corresponds to jumps of the tip between successive minima of $U(x)$, due to elastic instabilities induced by the driving spring ($\partial U / \partial x = 0$, $\partial^2 U / \partial x^2 = 0$). Close to the inflection point the height of the barrier preventing the tip sliding decreases with increasing applied force as $\Delta E \propto (\text{const} - F)^{3/2}$ [18–20]. This type of externally induced topological change in the free energy landscape is known as a fold catastrophe, and it has been found in many driven systems, including superconducting quantum interference devices [21, 22], mechanically deformed glasses [23], and stretched proteins [24, 25]. The simulation results obtained for diverse systems show that the fold catastrophe scaling is accurate not only in the immediate vicinity of the inflection point but over reasonably large intervals of loads.

The possibility of slips of higher multiplicity (multiple-slip regime) occurs for larger values of $\eta > 4.604$ [15]. However, this is the necessary but not sufficient condition to observe multiple slips, since the dynamics depends also on the damping coefficient γ . In particular, one can distinguish between the overdamped regime of motion, $\gamma > (\eta K/m)^{1/2}$, where the tip jumps between nearest-neighbor minima of the potential, and the underdamped regime, $\gamma < (\eta K/m)^{1/2}$, where, for $\eta > 4.604$, the tip may perform multiple slips over a number of lattice sites and even overshoot the lowest well of the potential $U(x)$. In the latter case the minimal spring force reached during stick-slip oscillations is negative.

The elastic instability occurring for $\eta > 1$ results in a nonzero value of the low-velocity kinetic friction that is given by the energy drop from the point of instability to the next minimum of the potential divided by a [26]. For $\eta < 1$ this instability disappears and the friction is viscous, $F_k \rightarrow 0$ for $v \rightarrow 0$. The emergence of static

friction can be interpreted as the arousal of a saddle-node bifurcation as a function of η , realizing a sort of fold-catastrophe scenario [27].

In experiment, the effective value of the PT parameter η can be controlled by the variation of the normal load on the contact, which changes the potential corrugation U_0 more than the contact stiffness. FFM experiments at low normal loads indeed demonstrated smooth sliding with ultralow friction, connected to the absence of elastic instabilities [15, 28]. At higher loads instead, “atomic” stick-slip took place with the atomic periodicity of the substrate lattice, while increasing load further led to a multiple slip regime as predicted by the PT model, see Fig. 1c.

In real systems at *finite temperature*, hysteresis and dissipation must disappear in the zero-speed limit of sliding, where stick-slip instabilities are preempted by thermal fluctuations. This regime is sometimes termed “thermolubricity” [18, 19, 29–32]. The main aspects of thermal effects on friction were considered in the pioneering work of Prandtl [16]. Thermal effects can be incorporated into the PT model (1) by adding a thermal random force $\hat{f}(t)$ and the damping term $-m\gamma\dot{x}$ to the conservative force between the slider and substrate, so that the tip motion is described by the Langevin equation

$$m\ddot{x} + m\gamma\dot{x} = -\partial U(x, t)/\partial x + \hat{f}(t). \quad (2)$$

The random force should satisfy the fluctuation-dissipation theorem. As usual, it is chosen with zero mean $\langle \hat{f}(t) \rangle = 0$ and δ -correlated:

$$\langle \hat{f}(t)f(t') \rangle = 2m\gamma k_B T \delta(t-t'), \quad (3)$$

where k_B denotes the Boltzmann constant and T temperature. The random force and the damping term arise from interactions with phonons and/or other fast excitations that are not treated explicitly.

In the thermal PT model, (2) and (3), beside the PT-parameter η , thermal fluctuations bring out a new dimensionless parameter δ representing the ratio between the pulling rate v/a and the characteristic rate of thermally activated jumps over the potential barriers, $\omega_0 \exp(-U_0/k_B T)$, where ω_0 is the attempt frequency [32]. As a result, one should distinguish between two regimes of motion: (i) $\delta \ll 1$, regime of very low velocities or high temperatures (typically $v < 1$ nm/s at room temperature), where the tip has enough time to jump back and forth across the barrier, and (ii) $\delta \gg 1$, the stick-slip regime of motion, where thermal fluctuations only occasionally assist the tip to cross the barrier before the elastic instability is reached. In these two regimes the following expressions for kinetic friction have been suggested [18, 19, 32]:

$$F_k(v, T) = \alpha(T)v + O(v^3), \quad \delta \ll 1, \quad (4)$$

$$F_k(v, T) = F_0 - bT^{2/3} \ln^{2/3} \left(B \frac{T}{v} \right), \quad \delta \gg 1 \text{ and } v < BT. \quad (5)$$

Here F_0 is the athermal ($T = 0$) low-velocity limit of friction, $\alpha(T) \propto (K/\omega_0) \times (U_0/k_B T) \exp(U_0/k_B T)$ is the equilibrium damping experienced by the tip (note that

α is independent of the ad-hoc damping coefficient γ), and b, B are positive constants which depend on m, K, a, U_0 and γ but not on v and T . (4) describes the slow friction regime (thermolubricity) and corresponds to the linear-response regime, while (5) has been derived assuming that thermally activated depinning occurs in the vicinity of the athermal instability point. The velocity and temperature dependences of friction force predicted by (5) result from the fold catastrophe scaling of the potential barriers, $\Delta E \propto (\text{const} - F)^{3/2}$. In between the regimes described by (4) and (5) one should observe a logarithmic dependence of F_k on velocity. However, it is very difficult to distinguish between $[\ln(v)]^{2/3}$ and simple $\ln(v)$ behavior in experiments as well as in numerical simulations [33]. The logarithmic (or $[\ln(v)]^{2/3}$) regime can span several decades, until v becomes so large that the inertial or viscous-like effects set in. The $[\ln(v)]^{2/3}$ dependence of the average rupture force has been also found in single-molecule unbinding experiments where the energy landscape of complex biomolecules is probed by applying time-dependent forces [34].

The theoretical framework outlined above explained a number of FFM experimental results on single crystal surfaces [29, 30, 35]. Furthermore, the statistical distribution of friction forces was measured to match predictions from the PT model [36]. These results provide strong evidence that atomic stick-slip in FFM is attributable to thermally activated slip out of a local minimum as described by the PT model. Thermally activated stick-slip friction is seen in MD simulation at sufficiently low speeds only, which are so far achievable through accelerated MD [37]. At higher speeds, friction is mostly determined by dissipative athermal dynamical processes, which correspond to a fundamentally different regime of sliding. This limits severely the regime of validity of comparisons of the PT model with MD simulations.

(4) and (5) also predict that kinetic friction should decrease with increasing temperature [18, 19, 38]. Thermal excitations help overcome energy barriers and reduce the stick-slip jump magnitude, so that nanofriction should decrease with temperature provided no other surface or material parameters are altered by temperature [39]. Recent experimental results [40–43], however, strongly disagree with the predictions of (4) and (5). Friction forces exhibit a peak at cryogenic temperatures for different classes of materials, including amorphous, crystalline, and layered surfaces. Instead, the temperature and velocity dependence of the kinetic friction is well described by the multicontact model [42, 43].

Several generalizations of the original 1D PT model include considerations of:

- two-dimensional (2D) structure of surfaces that led to the introduction of frictional imaging of interfaces [44–47];
- coupling between normal and lateral motion of the slider [48, 49] that led to a new approach to control friction and wear by modulating the normal load [50, 51];
- flexibility of the AFM tip apex that led to a predictions of new regimes of motion exhibiting complex stick-slip patterns [52, 53].

3 The Frenkel-Kontorova Model

The basic model describing the sliding of crystalline interfaces is the 1D Frenkel-Kontorova (FK) model (Ref. [54] and references therein). First analytically treated in Ref. [55] and then independently introduced to describe dislocations in solids [56–58], the FK model found subsequently a broad area of application, in particular, in surface physics, where it is used to unravel the behavior of adsorbed monolayers.

The standard FK model Hamiltonian

$$H = \sum_{i=1}^N \left[\frac{p_i^2}{2m} + \frac{1}{2}K(x_{i+1} - x_i - a_c)^2 + \frac{1}{2}U_0 \cos \frac{2\pi x_i}{a_b} \right] \quad (6)$$

describes a 1D chain of N harmonically coupled “atoms” subjected to a sinusoidal potential, see Fig. 2. The first term in (6) is the kinetic energy of the chain, the second one describes the harmonic interaction of the nearest neighboring atoms with the elastic constant K and equilibrium distance a_c , and the last term is the interaction of the chain atoms with the periodic potential of magnitude U_0 and period a_b . Static friction is probed by driving all atoms with an extra adiabatically increasing force F until sliding initiates.

The success of the FK model is partly due to the relevance of its continuum limit, valid for large K , where the FK equations of motion reduce to the exactly integrable sine-Gordon (SG) equation, the solutions of which, in addition to linear waves (phonons), include the topological solitons (called “kinks”) and dynamical solitons (“breathers”). Tribological processes in the FK model are ruled by kinks. Consider the simplest case of the trivial commensurate ground state (GS), when the number of atoms N is equal to the number of minima of the substrate potential M , so that the dimensionless concentration $\theta = N/M = a_b/a_c$ is 1. In this case, adding (or subtracting) one atom results in a chain configuration with one kink (or antikink) excitation (more rigorously, kinks may be defined on the background of any *commensurate* GS; in what follows, $\theta = 1$ kinks will be indicated as “trivial” kinks, while for a general case we will use the term “superkinks”). After relaxation, the minimum-energy configuration corresponds to a local compression (or extension in the antikink case) of the chain. Kinks move along the chain far more easily than atoms because the activation energy ε_{PN} for kink motion [known as the Peierls-Nabarro (PN) barrier] is always smaller (or much smaller) than the amplitude U_0 of the substrate potential.

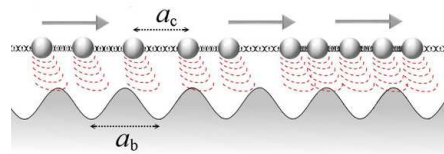


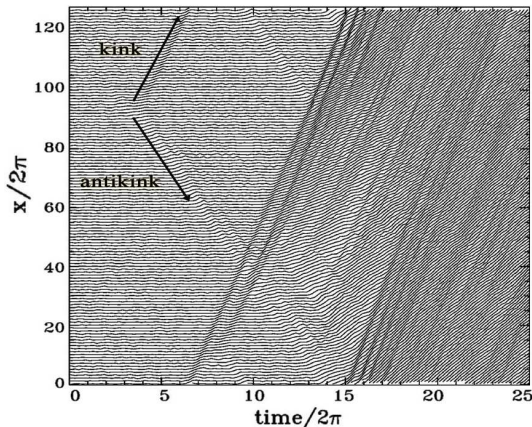
Fig. 2 A sketch of the FK model with the two competing lengths: interparticle and substrate periodicities.

Because the kinks (antikinks) are associated with extra atoms (vacancies), their motion provides a mechanism for mass transport along the chain so that they are responsible for mobility, conductivity and diffusivity. The higher the concentration of kinks, the higher is the system mobility [60]. When the GS is commensurate (e.g., $\theta = 1$), the first step to initiate motion in the FK model is the (e.g. thermally induced) creation of a kink-antikink pair, see Fig. 3.

When the elastic layer is of finite extension, kinks are usually generated at a free end of the chain and then propagate along the chain until disappearing at the other free end [61]. Each run of the kink through the chain results in the shift of the whole chain by one lattice constant a_b . In the case of a finite film confined between two solids, one may similarly expect that the onset of sliding is initiated by the creation of a kink at the boundary of the contact. Subsequent kink motion is the basic mechanism of sliding. In 2D or three-dimensional (3D) systems, concepts of domain walls or misfit dislocations are used instead of kinks, but the physics of these processes remains qualitatively the same.

A crucial role in the FK model is played by incommensurability. Let the substrate period a_b and the natural period of the chain a_c be such that, in the limit of an infinite system's length, their ratio $\theta = a_b/a_c$ is irrational. In this case, under a not too restrictive condition on θ [62], there exists a critical value of the elastic constant K , such that for a higher rigidity the chain becomes effectively free of the substrate, i.e., the static friction F_s drops to zero, and the kinetic friction becomes very small. This phenomenon is known in physics from the beginning of the 1970s as the commensurate-incommensurate transition, or (later on, when S. Aubry developed the rigorous mathematical theory) “the transition by breaking of analyticity”, or simply the *Aubry transition* [63–68]. A simple explanation of the $F_s = 0$ sliding state is the following: in this state, for every atom going up over the barrier, there is

Fig. 3 Atomic trajectories as a function of time of the perfectly commensurate ($\theta = 1$) FK chain at the depinning transition, at a small temperature. The onset of motion is marked by the nucleation of a kink-antikink pair. The kink and antikink move in opposite directions, collide quasielastically (because of the periodic boundary conditions), and soon a second kink-antikink pair is created in the tail of the primary kink. This process repeats with an exponential (avalanche-like) growth of the kink-antikink concentration, leading to a sliding state. (Adapted from [59])



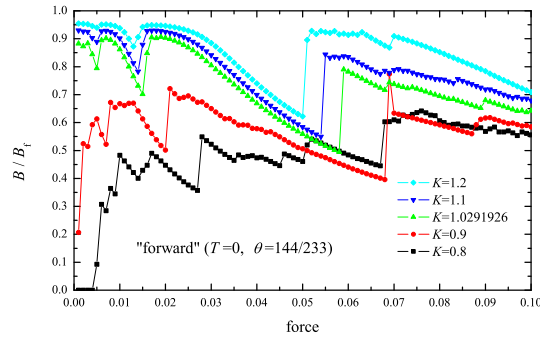
another atom going down, and the energy costs of these processes compensate exactly each other. Roughly speaking, the incommensurate FK chain acquires a “staircase” deformation, with regions of approximate commensurability separated by regularly spaced superkinks. If there is a nonzero probability to find atoms arbitrarily close to the maximum potential energy U_0 these superkinks are unpinned and mobile, otherwise they are pinned [69]. For a fixed value of U_0 , the FK GS undergoes a transition between these two states at a critical value $K = K_c$ of the chain stiffness. The value K_c depends dramatically and discontinuously on the incommensurability ratio a_b/a_c defining the interface; it takes the minimal value $K_c \approx 1.0291926$ [in units of $2U_0(\pi/a_b)^2$] for the irrational golden mean ratio $a_b/a_c = (1 + \sqrt{5})/2$ [54]. For $K > K_c$ there is a continuum set of ground states that can be reached adiabatically through nonrigid displacements of chain atoms at no energy cost (*the sliding mode*, or *the Goldstone mode*). On the other hand, for $K < K_c$, the atoms are trapped close to the minima of the substrate potential and thus require a finite energy to move over the corrugated substrate. Thus, for the incommensurate contact above the Aubry transition ($K > K_c$) chain sliding is initiated by even the smallest driving force and, accordingly, the static friction force vanishes, $F_s = 0$. On the contrary, for K below K_c the two incommensurate 1D surfaces are locked together due to pinning of the superkinks that separate local regions of common periodicity, and in this case we expect stick-slip. Note also that a finite-size FK chain is always pinned, even for an irrational value of a_b/a_c because of the locking of the free ends of the chain (although an Aubry-like transition, exhibiting a symmetry-breaking nature, can still be defined [70–72]).

In order to characterize the Aubry transition, it is convenient to introduce a “disorder” parameter ψ defined as the minimum distance of any atom from the nearest top of the substrate potential. Near the critical point the transition from pinned to sliding ground states occurs according to a power law,

$$\psi \propto (K_c - K)^{\chi_\psi}, \quad F_s \propto \varepsilon_{PN} \propto (K_c - K)^{\chi_{PN}}, \quad (7)$$

where the critical exponents χ depend on the incommensurability ratio, in particular, for the golden-mean case $\chi_\psi \approx 0.7120835$ and $\chi_{PN} \approx 3.0117222$ [68, 73–79].

Fig. 4 The mobility $B = v/F$ normalized to the free-motion value $B_f = (m\gamma)^{-1}$ as a function of the dc force F for the classical FK model with the “golden-mean” concentration for different values of the elastic constant K below and above the Aubry threshold $K_c \approx 1.0291926$. The equation of motion included an external viscous damping, with a friction coefficient $\gamma = 0.1$. (Adapted from [54])



Notice that the Aubry transition exhibits a scaling behavior as typical for critical phenomena. The exponents in (7) are called super-critical because they only apply to the locked side of the transition, $K \leq K_c$.

Likewise, one may introduce also sub-critical exponents for the sliding state above the Aubry transition. An important subcritical quantity is the effective viscosity $\Gamma = \lim_{F \rightarrow 0} F/(m\nu)$ which describes the steady-state average velocity ν in response to an infinitesimally small dc force F applied to all atoms (to avoid infinite acceleration, an external damping γ should be included in the equation of motion). Γ is zero in the SG limit ($K \rightarrow \infty$) and diverges at the Aubry transition. For the golden-mean concentration, Γ scales as

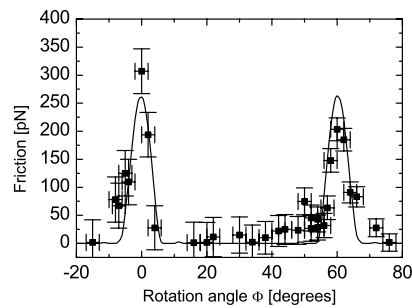
$$\Gamma(K) \propto (K - K_c)^{-\chi_\Gamma} \quad (8)$$

with $\chi_\Gamma \approx 0.029500$. The scaling (8) is only appropriate immediately above the Aubry transition, while at $K \gg K_c$, Γ decreases toward γ . Accordingly, for any $K > K_c$ the mobility $B = \nu/F$ remains lower than its maximum value $(m\gamma)^{-1}$ even in the $F \rightarrow 0$ limit as illustrated for $K \gtrsim K_c$ in Fig. 4. A “frictionless” motion of the truly incommensurate GS exists only in the SG ($K \rightarrow \infty$) limit, where the substrate-corrugation U_0 term adds no dissipation to the one brought in by the γ term.

Vanishing static friction has been first found within the FK model for mutually incommensurate periodicities and sufficiently hard infinite lattices [68]. Later on [80–82], this effect was predicted for infinite incommensurate contacts, and called *superlubricity*. The term superlubricity has been criticized as misleading, since it might wrongly suggest null friction in the sliding state in analogy to superconductivity and superfluidity. Instead, incommensurability of periodic interfaces cancels only one of the channels of energy dissipation, that originating from the low-speed stick-slip elastic instability. Other dissipative processes, such as the emission of sound waves, still persist, and therefore even in the case of complete incommensurability the net kinetic friction force does not vanish, although in the superlubric regime one expects a substantial reduction of the friction force relative to a similar, but commensurate case.

Detailed experimental studies of superlubricity have been performed recently for friction between a graphite flake attached to the FFM tip and an atomically

Fig. 5 The data points show the average friction force versus the rotation angle measured by [83]. The curve through the data points shows the calculated friction force from a PT-like model for a symmetric 96-atom flake. (Reproduced from [84])



flat graphite surface [83–85]. Super-low friction forces (< 50 pN) were found for most relative orientations of the flake and the substrate, for which the contacting surfaces find themselves in incommensurate states (see Fig. 5). For narrow ranges of orientation angles corresponding to commensurate contacts, stick-slip motion was observed and friction was high (typically 250 pN).

The kinetic friction properties of the FK model [86, 87] are probed by adding a (e.g. Langevin) thermostat as described for the PT model above. Even above the Aubry transition, where $F_s = 0$, the kinetic friction force F_k is nonzero, because the dynamics at any finite speed results in the excitation of phonons in the chain. At finite T , pinning can be overcome by thermal fluctuations, which can initiate sliding even in the most-pinned state, the fully commensurate one, see Fig. 3. Finally, we remark that friction in the dynamically driven FK model describes fairly the onset of sliding of a crystalline contact [88], but it cannot account for the highly inelastic plastic or quasi-plastic deformations of the surfaces characterizing real-life friction experiments.

The dimensionless atomic concentration $\theta = N/M = a_b/a_c$ in the FK system plays a crucial role since it defines the concentration of “geometrical” superkinks. As mentioned above, these excitations can be defined for any background *commensurate* atomic structure $\theta_0 = p/q$, where p and q are relative prime integers. If the concentration θ slightly deviates from the background value θ_0 , the GS of the system corresponds to large domains with background commensurate structure θ_0 , separated by localized incommensurate zones of compression (expansion) called superkinks (super-antikinks).

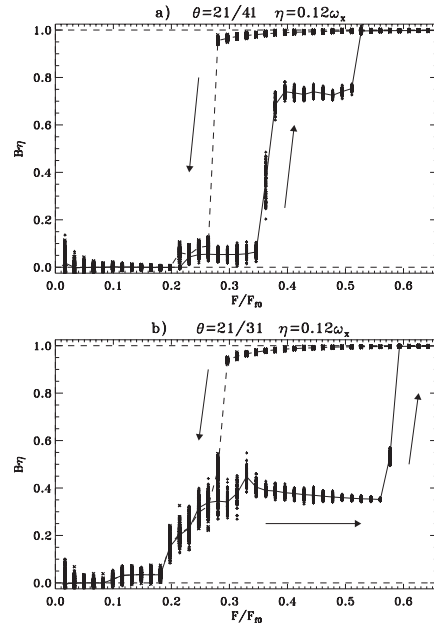


Fig. 6 The mobility $B = v/F$ versus the force F for the underdamped ($\gamma = 0.12$) FK model with exponential interaction ($K_{\text{eff}} = 0.58$) (a) for $\theta = 21/41$ (superkinks on the background of a $\theta_0 = 1/2$ structure), and (b) for $\theta = 21/31$ (superkinks on the background of the complex $\theta_0 = 2/3$ structure). (Reproduced from [89])

When the external force increases, the FK system with a non-trivial GS exhibits a hierarchy of first-order dynamical phase transitions from the completely immobile state to the totally running state, passing through several intermediate stages characterized by the running state of collective quasiparticle excitations, or kinks of the FK model. As an example, let us consider the $\theta = 21/41$ case when the mass transport along the chain is carried out by trivial kinks constructed on the background of the $\theta_0 = 1/2$ structure. As the average distance between the kinks is large (equal to $41 a_b$ in the GS), the kink-kink interaction is weak, and the atomic flux is restricted by the overcoming of kinks over the PN barriers (see Fig. 6a). When the driving force F increases, the now-tilted effective PN barriers are lowered (simultaneously with the original barriers of the substrate potential), resulting in the increase of the single-kink mobility. Thus, at zero temperature the crossover from the locked $B = 0$ state to the kink-running state takes place at the force $F \approx F_{tk} = C\pi\epsilon_{PN}/a_b$, where the factor $C \sim 1$ depends on the shape of the PN potential. The mobility in the kink-running state is $B \approx \theta_k B_f$, where $\theta_k = 1/41$ is the dimensionless kink concentration.

The further scenario depends on the value of the damping coefficient γ . At very low damping, $\gamma < 0.05$, there is no intermediate stages, because the running kinks destroy themselves as soon as they start to move: they will cause an avalanche driving the whole system to the totally running state of atoms similarly to that shown in Fig. 3. At larger damping, $\gamma > 0.05$, the above-mentioned intermediate stages with running kinks exist. A mechanism of the second abrupt increase of the mobility depends on γ too (for details see [54, 89, 90]). Between the kink-running stage and the totally running state there may be a specific “traffic-jam” regime [54].

This qualitative picture holds also for a more complex atomic structure like $\theta = 21/31$ [89] (see Fig. 6b for $N = 105$ and $M = 155$). In this case the state of running trivial kinks is preceded by the state of running superkinks. The GS in this case corresponds to domains of the complex $\theta_0 = 2/3$ commensurate structure, separated by *superkinks* with an average spacing $30 a_b$ between them. On the other hand, the $\theta = 2/3$ structure can be viewed as a dense lattice of *trivial* kinks defined on the background of the $\theta_0 = 1/2$ structure. This specificity clearly manifests itself in the $B(F)$ dependence. During the force-increasing process, there are now two sharp steps of increasing of the mobility B . The first one, at $F = F_{sk} \approx 0.08 F_s$, corresponds to the situation where the superkinks start to slide, whereas the second step, occurring at $F = F'_{tk} \approx 0.18 F_s$, corresponds to the transition of the trivial kinks to the running state.

3.1 Extensions of the Frenkel-Kontorova Model

Many relevant generalizations of the FK model have been proposed so far to cover a large class of frictional relevant phenomena. They mainly consist of modifications of model interactions or of dimensionality. For realistic physical systems, anharmonicity can be introduced in the chain interatomic potential, see Ref. [54]. The main novelties here include effects such as a broken kink-antikink symmetry, new

types of dynamical solitons (supersonic waves), a possible breakup of the antikink soliton followed by a chain rupture, and a modified kink-kink interaction. Strong anharmonic effects are responsible of a strong kink-antikink asymmetry in recent experiments of friction in repulsive colloids [91,92], see chapter ?? . Likewise, non-sinusoidal periodic substrates, characterized, e.g., by sharp bottoms and flat barriers [93], have been investigated to address atoms adsorbed on a metal surface. Complex unit cell substrates [60,94], as well as quasiperiodic [95,96] and disordered corrugated profiles [97–99] have also been considered. These deviations from the standard FK model may lead to qualitatively different excitations such as different types of kinks, phonon branches, and to changes in the kink-antikink collision scenario. From a tribological point of view, different types of sliding behavior are to be expected at low-driving forces, when the dynamics is mainly governed by the motion of kink-like structures.

A very important generalization of the standard FK chain with relevant consequences for the tribological properties (critical exponents, scaling of friction force with system size, mechanisms of depinning, etc.) involves increasing the dimensionality of the model. Especially the 2D generalized versions of the FK model [11,54] are naturally applicable to the description of a contact of two crystalline surfaces (i.e., the case of “dry” friction), in particular as is realized in QCM experiments, where 2D monoatomic islands of adsorbate atoms slide over a periodic crystalline substrate [8], or, very recently, in 2D colloidal monolayers over laser-generated optical lattices [91,92,100,101]. Among 2D generalized FK models we mention the model consisting of two coupled FK chains [102], the 2D “springs and balls” FK model describing a 2D layer of harmonically interacting atoms in the 2D periodic substrate, the scalar anisotropic 2D FK model treating a system of coupled 1D FK chains, the vector anisotropic 2D FK model (e.g., the zigzag FK model), the vector isotropic 2D FK model [103–106], and the 2D tribology model [88,107] (see also [54] and references therein).

The approaches based on these models are especially powerful in the investigation of the transient behavior at the onset (or stopping) of sliding, which is quite difficult to study in fully realistic 3D models (e.g., see [108]). As a typical example, let us describe the onset of sliding observed in the vector 2D FK model, where a 2D layer of atoms is subjected to a periodic substrate potential with the triangular symmetry [108]. The transition from the locked to running state is mediated by the formation of an island of moving atoms in a sea of essentially stationary particles. The size of the moving island grows quickly in the direction of the driving force, and somewhat more slowly in the perpendicular direction. Inside the island the atoms largely maintain their triangular structure due to the stiffness of the atomic layer. Hence one sees areas of essentially perfect triangular lattice surrounded by a closed boundary of partial dislocations. In simulation, due to periodic boundary conditions, the island eventually joins up on itself. There forms a strip (“river”), oriented parallel to the driving force and bounded in the direction perpendicular to the driving force, in which particles move along the periodically-continued system. Outside this stripe the particles are immobile. This stripe then broadens perpendicularly to the driving

direction until all atoms are moving. The evolution of this scenario is illustrated in a series of snapshots in Fig. 7.

Noncontact AFM tips oscillating on top of kink-like adsorbate regions [109] dissipate significantly more than nearly in-registry regions. This mechanism is explained by the higher softness and mobility of solitonic regions [110–113], and it has been demonstrated by the dynamics of an incommensurate FK chain, forced and probed by a locally-acting oscillation [114].

In investigating *confined* systems under shear, FK-like models with just one particle [115–117] or an interacting atomic chain [118–120] embedded between *two* competing substrates have led to uncover peculiar tribological phenomena related to stick-slip dynamics or to the appearance of remarkable sliding regimes of motion. For example, velocity quantization phenomena have been reported [121, 122] in the motion of an idealized 1D solid lubricant.

In slider-lubricant-slider geometry [120] sketched in Fig. 8c, the lattice mismatch can give rise to peculiar and robust “quantized” sliding regimes, characterized by a nontrivial geometrically fixed ratio of the mean lubricant drift velocity and the externally imposed translational velocity. In detail, the speed ratio $w = v_{cm}/v_{ext}$ remains pinned to exact “plateau” values over wide ranges of parameters, such as sliders corrugation amplitude, external velocity, chain stiffness and dissipation (see Fig. 8a), and is strictly determined by the length ratios alone. The plateau mechanism has been interpreted in terms of solitons, formed by the mismatch of the lubricant periodicity to that of the nearer matching substrate, being rigidly dragged forward by the advancing sinusoid representing the other, more mismatched, slider.

The finding of exact plateaus implies a kind of “dynamical incompressibility”, namely identically null response to perturbations or fluctuations trying to deflect the CM velocity away from its quantized value. In order to probe the robustness of the plateau attractors, an additional constant force F_{ext} , acting on all particles in

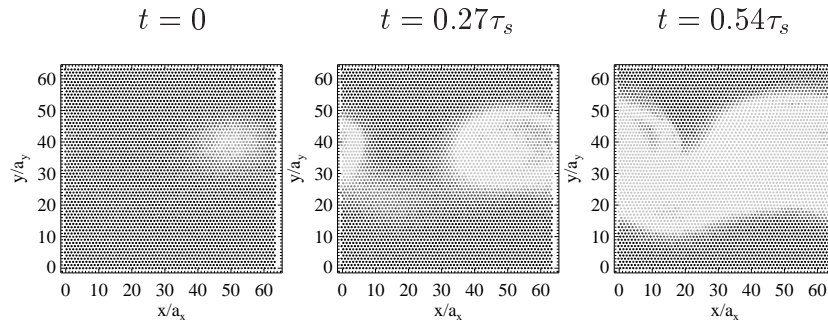


Fig. 7 Successive snapshots of the mechanism of the locked-to-running transition in the vector 2D FK model for the LJ interaction with $K_{eff} = 0.9$, $\gamma = 0.141$, $T = 0.05$, and $F = 0.9933$. The positions of the atoms are indicated by circles. The x component of the particle speed is shown in grey scale: from zero (black) to maximum (lightest grey) velocity. (Adapted from [108])

the chain, was introduced. As expected, as long as F_{ext} remains sufficiently small, it has no effect whatsoever on the velocity-plateau attractor. The plateau dynamics is only abandoned above a critical force F_c . The transition, occurring for increasing external driving force F_{ext} acting on the lubricant, displays a large hysteresis, and has the features of depinning transitions in static friction, only taking place “on the fly” [123, 124]. Although different in nature, this phenomenon appears isomorphic to a static Aubry depinning transition [67, 68], the role of particles now taken by the moving solitons of the lubricant-substrate interface. The confined model was extended beyond the standard sinusoidal corrugation of (6): the quantized velocity remains, but a nonsinusoidal corrugation can affect the parametric region where the velocity plateau extends [125].

A quantized sliding state of the same nature has been demonstrated by MD simulations for a substantially less idealized two-dimensional model [126], where atoms of a lubricant multilayer film were also allowed to move perpendicularly to the sliding direction and interact via Lennard-Jones potentials (see Fig. 9). This dynamical regime, is shown to be robust against the effects of thermal fluctuations, quenched disorder in the confining substrates, and over a broad range of loading forces. By

Fig. 8 (a) The average drift velocity ratio $w = v_{cm}/v_{ext}$ of the chain as a function of its lubricant stiffness K for different commensurability ratios (r_+, r_-) , with $r_{\pm} = a_{\pm}/a_0$: commensurate $(3/2, 9/4)$, golden mean (GM) (ϕ, ϕ^2) ($\phi \simeq 1.6180\dots$), spiral mean (SM) (σ, σ^2) ($\sigma \simeq 1.3247\dots$), and (ϕ^{-1}, ϕ) . The (ϕ, ϕ^2) 1/1 plateau value is $w = 0.381966\dots$, identical to $1 - \phi^{-1}$ to eight decimal places. (b) The main plateau speed w as a function of r_+ . (c) A sketch of the model. (Reproduced from Ref. [121])

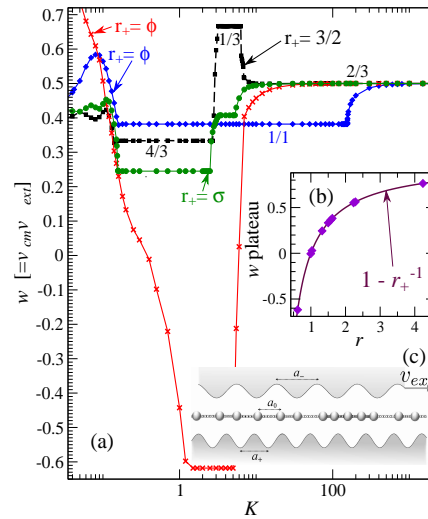
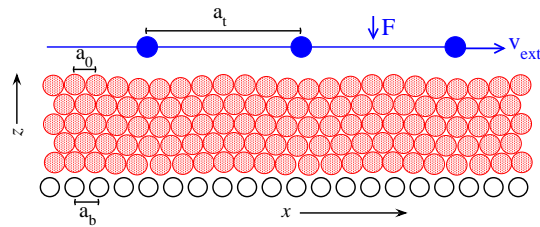


Fig. 9 A sketch of the model with rigid top (solid circles) and bottom (open) layers (of lattice spacing a_t and a_b respectively), the former moving at externally imposed x -velocity v_{ext} . One or more lubricant layers (shaded) of rest equilibrium spacing a_0 are confined in between. (Reproduced from Ref. [126])



evaluating its tribological properties in terms of averaged kinetic friction \overline{F}_k exerted on the top slider, this lubricant quantized sliding has been found [127] to be characterized by significantly low values of \overline{F}_k , see Fig. 10.

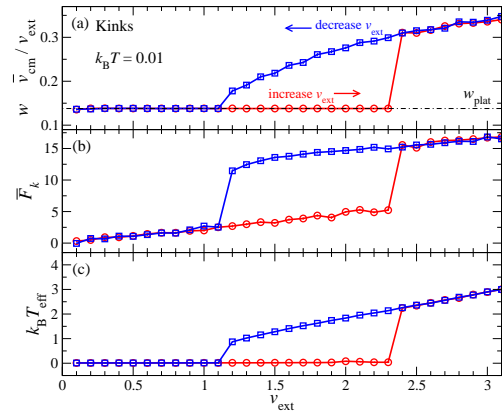
While certain of these phenomena, such as chaotic and inverted stick-slip motion, two types of smooth sliding and transitions between them, have already been observed [128, 129], others are still waiting for experimental confirmation.

Last but not least, the combined Frenkel-Kontorova-Tomlinson (FKT) model [130, 131] has been introduced including harmonic coupling of the interacting chain atoms to a sliding body. The FKT model introduces more degrees of freedom than the PT model, and it has been used to describe effects of finite size and stiffness of the AFM tip and of normal load on friction [132, 133]. The latter effect has been modeled assuming that the amplitude U_0 of potential corrugation increases proportionally to the applied normal force. The validity of the FKT model has been tested by 3D MD simulations [133], which confirmed the outcome of the model for most investigated regimes except for the limit of very low stiffness and high normal load. Unlike the FKT model where the breakdown of superlubricity coincides with the emergence of the metastable states, in 3D simulations certain metastable states appear to reduce the frictional force leading to nonmonotonic dependence of force on normal load and tip compliance. Increasing dimensionality and adding realistic features to the FK model brings its extensions into closer and closer contact to full-fledged MD simulations.

4 Molecular Dynamics Simulations

The simple low-dimensional MMs discussed above are useful for a qualitative understanding of many physical aspects of friction. To address subtler features of a specific interface, one should go beyond MMs including atomistic structural details of the interface. Such an approach is provided by MD simulations.

Fig. 10 As a function of the adiabatically increased (circles) or decreased (squares) top-substrate velocity v_{ext} , the three panels report: (a) the average velocity ratio w ; (b) the average friction force experienced by the top substrate; (c) the effective lubricant temperature, computed using the average kinetic energy in the frame of reference of the instantaneous lubricant center of mass. (Reproduced from Ref. [127])



Advances in computing hardware and methodology have dramatically increased our ability to simulate frictional processes and gather detailed microscopic information for realistic tribological systems. MD simulations represent controlled computational experiments where the dynamics of all atoms is obtained by solving numerically Newton or Langevin equations of motion based on suitable interparticle interaction potentials and the corresponding interatomic forces. The geometry of the sliding interface and the boundary conditions (e.g. as sketched in Figs. 11 and 12) can be chosen to explore friction, adhesion and wear.

A worthwhile guide to atomistic MD simulations of frictional processes focusing on fundamental technical aspects (realistic construction of the interface, appropriate ways to impose load, shear, and the control of temperature) can be found in the review articles by [135,136]. By following the Newtonian dynamics of a system executing sliding for a significant amount of time, quantities of physical interest such as instantaneous and average friction force, mean (centre-of-mass) slider velocity, heat flow, and correlation functions are numerically evaluated. Unlike standard equilibrium MD simulations of bulk systems, frictional modeling inherently involves non-equilibrium conditions and a nonlinear dissipative response to the external driving. A standard practical assumption is to add Langevin terms to Newton's equations, like in (2) and (3) for the PT model at finite temperature.

The choice of the appropriate interaction forces between atoms represents a major problem. If $U\{R_1, R_2, \dots, R_N\}$ is the total energy of the system as a parametric function of all atomic coordinates $\{R_i\}$, the force on atom i is $F_i = -\nabla_{R_i} U$, perfectly determined once U is known. Unfortunately, this is generally not the case, because U is determined by the quantum mechanics of electrons — a much bigger and unsavory problem to solve. *Ab-initio* MD, e.g. of the Car-Parrinello type [137], has not really been of use so far in sliding friction, mainly because it can handle only rather small systems, typically hundreds of atoms, for relatively short times, typically $\ll 1$ ns. Most MD frictional simulations are therefore based on reasonable empirical interatomic forces (“force fields”), ranging from relatively sophisti-

Fig. 11 Sketch of a typical MD simulation of a boundary-lubricated interface under shear. Periodic boundary conditions are applied in the x - y directions.

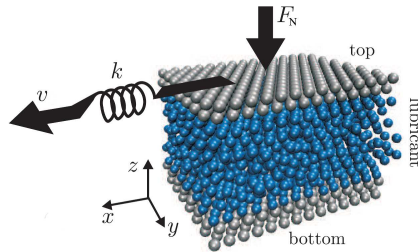
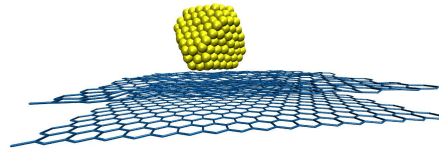


Fig. 12 A simulated truncated-octahedron Au_{459} cluster sliding with one of its (111) facets over a mobile graphite substrate. (Reproduced from [134]).



cated energy surfaces accounting for electrons at the density-functional level or at the tight-binding level [138], to angle-dependent many-particle potentials, to simple pairwise potentials (e.g. Lennard-Jones or Morse), to basic simple models of elastic springs which represent extensions of FK-type formulations. In practice, several reliable force fields, parameterized to fit different ranges of experimental data and material combinations, are available in the literature [139–143]. While this allows qualitative atomistic simulations of sliding friction, it is often far from quantitative. For example, during such a violent frictional process as wear, atoms may change substantially their coordination, their chemistry, sometimes their charge. Once a specific system is understood after the elaborate development of satisfactory potentials, the mere change of a single atomic species may require a complete reparametrization of the interatomic forces. As a result, systematic frictional studies may become quite a challenge in the absence of a consistent set of potentials. A promising approach consists in the use of the so-called reactive potentials [144–146], capable of describing chemical reactions and interface wear, with the advantage, for large-scale atomic simulations, of a good computational efficiency compared to first-principle and semi-empirical approaches.

4.1 Thermostats and Joule Heat

In a tribology experiment, mechanical energy is converted to Joule heat which is carried away by phonons (and electron-hole pairs in metals). In a small-size simulation, the excitations generated at the sliding interface propagate and crowd-up into an excessively small region of “bulk” substrate, where they are back-reflected by the cell boundaries, rather than properly dispersed away. To avoid overheating and in order to attain a frictional steady state, the Joule heat must therefore be steadily removed. If this removal is done by means of standard equilibrium thermostats such as velocity rescaling or Nosé-Hoover or even Langevin dynamics, an unphysical dissipation is distributed throughout the simulation cell, so that simulated atoms do not follow their real conservative motion, but rather execute an unrealistic damped dynamics which turns out to affect the overall tribological properties [147]. Similarly in the PT and FK models, the damping parameter γ is known to modify kinetic and frictional properties, but there is no clear way to choose the value of γ .

To solve this problem, one should attempt to modify the equations of motion inside a relatively small simulation cell so that they reproduce the frictional dynamics of a much larger system, once the remaining variables are integrated out. One approach is to use in Langevin equations a damping coefficient which depends on the coordinate and velocity of each lubricant atom; these dependences can be taken to fit the known dissipation of atoms adsorbed on a surface [148]. In turn, this method requires a modification of the standard Langevin technique [149]. A more rigorous approach is a recent implementation of a non-conservative dissipation scheme, based on early formulations by [150–152] and subsequent derivations by [153–155], that has demonstrated the correct disposal of friction-generated phonons, even in the

relatively violent stick-slip regime [156, 157]. All atoms near the sliding interface follow plain Newton's equation, while the atoms in the deepest simulated layer, representing the boundary layer in contact with the semi-infinite heat bath, acquire additional non-conservative (and non-Markovian) terms which account for the time history of this layer through a memory kernel [153, 154]. Nanofriction simulations exploiting this dissipative scheme have recently been implemented that conceptually and practically improve over a traditional Langevin simulation.

4.2 Size- and Time-scale Issues

Modern CPUs perform of the order of 10^9 floating-point operations per second (FLOPS) per core. Classical MD can take advantage of medium-scale parallelization, with fairly linear scaling to approximately 10^2 cores, thus affording about 10^{11} FLOPS. As the calculation of the force acting on each atom (usually the dominating step in a MD calculation) can require, depending on the complexity and range of the force field, 10 to 10^2 operations, the product of the number of simulated particles N times the number of time-integration steps N_{step} per runtime second on a modern medium-size parallel computer is approximately $NN_{\text{step}} \simeq 10^{10}$. With a typical time-step of ~ 1 fs, a medium-size simulation involving $N = 10^5$ atoms can progress at a rate of 10^5 fs per second, i.e. approximately 10^9 fs = $1 \mu\text{s}$ in a simulation day. This total time scales down for larger systems sizes.

These estimates should be compared with the typical times, sizes, and speeds of tribology experiments. If we wish to address macroscopic sliding experiments, the speed would be in the 0.1 to 10 m/s range: in $1 \mu\text{s}$ the slider advances by 0.1 to $10 \mu\text{m}$, i.e. approximately 10^3 to 10^4 typical lattice spacings, enough for a fair statistics of atomic-scale events (but hardly sufficient to gather significant data about phenomena such as the diffusion of additives or of wear particles within the lubricant, or step- or defect-related phenomena). In a nanoscale FFM experiment, however, the tip advances at a far smaller average speed (i.e. $\simeq 1 \mu\text{m/s}$) and we can simulate a miserable $\simeq 1$ pm advancement in a typical run, far too short to observe even a single atomic-scale event, let alone reaching a steady state. Therefore, whenever long-distance correlations and/or slow diffusive phenomena and/or long equilibration times are expected, MMs will perform better than fully atomistic MD simulations. There is nevertheless so much physical insight to be extracted from MD simulations that it makes sense to run them even at larger speeds than in AFM or SFA experiments; and indeed, the sliding speed adopted in most current atomistic MD frictional simulations is in the m/s region.

While the high-speed kinetic friction is reproduced adequately in MD simulation, it is not so for the static friction which essentially depend on the system size, usually decreasing with the increase of the interface area. To overcome this problem, one may use scaling arguments which allows to find the large-area static friction from MD simulation for a rather small system [158].

One of the challenging problems for MD simulations is to account for the transition from stick-slip to steady sliding. In SFA and AFM experiments, stick-slip with its associated hysteresis and large friction generally disappears for speeds larger than $\sim 1 \mu\text{m/s}$, while in MD simulations the transition takes place in the m/s range. This major discrepancy (up to ~ 6 orders of magnitude in speed!) between simulations and experiments has been discussed [159–162], and relates to the effective spring-force constants and mass distributions, that are hugely different in the two cases, and much oversimplified in simulations. Several attempts to fill these gaps rely on methods, including hyperdynamics, parallel-replica dynamics, temperature-accelerated dynamics, and on-the-fly kinetic Monte Carlo devised in recent years [163–165].

Another important aspect present in experiments and largely missed by MD simulations is the ageing of contacts due to the interface relaxation. Contact ageing is believed to be responsible for the increase of the static friction force as a function of the contact time. Direct imaging of contact regions in samples under a normal load shows a logarithmic growth with time [166], leading therefore to a slowly increasing static friction. At the phenomenological level, frictional ageing is well described by rate and state friction laws, widely used in geophysics [167], but its microscopic origin is still debated. The main mechanisms that have been invoked in the past to explain it are plastic creep [168] or chemical strengthening at the interface [169]. In a recent paper [169], AFM was used to explore ageing in nanoscale contact interfaces, finding supporting evidence for the second mechanism, since when the contact surface was passivated it showed no ageing. It is however likely that at larger scales and loads plastic creep would also play an important role. Beyond its direct relevance for friction, the intriguing issue of contact ageing occurs in other non-equilibrium disordered systems such as granular media or glasses.

4.3 *Multiscale Models*

Since it is currently impossible to treat atomistically all the characteristic length scales that mark the dynamical processes entering the friction coefficient of engineering materials, a rising effort is nowadays devoted to develop multiscale approaches. The basic consideration is that unless conditions are very special, all processes far away from the sliding interface can be described approximately by continuum mechanics and simulated using finite elements, allowing for a macroscopic description of elastic and plastic deformation. The advantage of these continuum-theory methods is that it is possible to increasingly coarse-grain the system as one moves away from the sliding contact, thereby highly reducing the computational effort. Several groups [170, 171] combine the atomistic treatment of the interfacial mating region, where displacements occur on an atomic or larger length scale, with a coarse-grained or finite-element continuum description elsewhere, where strains are small and continuous. The main difficulty lies in the appropriate matching conditions between the atomistic and continuum regions [172]. Since the detail of lattice vibrations (the phonons), which are an intrinsic part of any atomistic model, can-

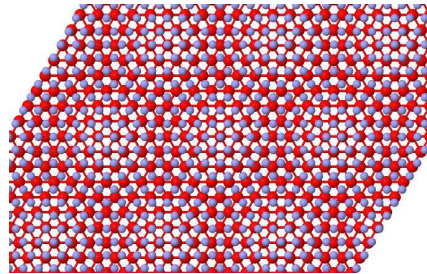
not be fully represented at the continuum level, conditions must be met that at least the acoustic phonons should not be reflected excessively at the atomistic-continuum interface. In other words, matching at this interface must be such that sound deformations transmit with reasonable accuracy in both directions, which is vital to a proper account of Joule-heat disposal into the bulk. Chapter ?? covers this issue.

4.4 Selected Results of MD Simulations

Here we survey some results from the growing simulation literature, certainly not providing an adequate review of the field. With two sliding surfaces separated by a thick fluid film, friction is mainly determined by the lubricant viscosity. The friction coefficient can be calculated using the Navier-Stokes equations, showing a monotonic increase with the relative sliding velocity [173]. For small driving velocity and/or high load, the lubricant cannot usually keep the surfaces apart and solid-solid contact eventually ensues. But even before full squeezeout, a liquid confined within a nanometer-scale gap ceases to behave as a structureless fluid — it becomes layered and even may solidify when thickness decreases below about five molecular layers. Pioneering studies of confined systems under shear reveal a sequence of drastic changes in the static and dynamic properties of fluid films in this “boundary-lubrication” regime.

SFA experiments [174] and MD simulations [175, 176] have both shown clear upward frictional jumps, in correspondence to squeezeout transitions from N to $N - 1$ lubricant layers. The lubricant squeezeout for increasing load becomes harder and harder, corresponding to a (near) crystallization of the initially fluid lubricant [177–179]. But friction would not necessarily always jump upward during the layer-by-layer squeezeout: it could jump downward as well, if lattice mismatch between the compressed boundary lubricant layer and the rigid substrates jumped from

Fig. 13 (color online). Top view of a snapshot of a 3D MD simulation of the solitonic pattern arising at the boundary layer of a solid lubricant (light grey) in contact with a perfect crystalline surface (dark/red), induced by a 16% lattice-constant mismatch. The Lennard-Jones interaction of this simulation favors in-registry hollow sites, while unstable top sites mark solitonic regions. Other layers were omitted for clarity.



commensurate to incommensurate, the latter superlubric with a mobile soliton pattern, as sketched in Fig. 13.

MD investigations of a melting-freezing mechanism in the stick-slip phenomenology of boundary-lubricated films were carried out by [180–183]. Various realistic models for lubrication layers in very specific contexts have been investigated with extensive MD simulations [162, 184–187]. During sliding, a thin lubricant film may be solid or liquid, depending on the interplay between the strength of interaction of lubricant molecules with the surfaces and between themselves. In the case of weaker interaction with the surfaces, the sliding takes place at the lubricant-surface interface, and the lubricant film remains in the solid state. And if the substrate and the solid lubricant both have near-ideal crystalline structures and these structures are incommensurate, superlubric sliding with zero static friction and very low kinetic friction ensues: the solid lubricant may provide minimal friction coefficient. But in practice the surfaces, as well as the lubricant, are unlikely to retain undefected crystalline structures. The presence of impurities or defects between the sliding surfaces can, even in a relatively small concentration, leads to pinning and nonzero static friction [188], thus destroying superlubricity. However, if one carefully chooses the parameters of the lubricant, the perfect sliding could again be achieved, because the lubricant may self-order itself during sliding [189].

In the opposite case of a strong interaction of lubricant molecules with the surfaces, the latter are covered by lubricant monolayers which protect surfaces from wear, and sliding occurs somewhere in the bulk of the lubricant film. In this case the film usually melts during sliding (a thin lubricant film, however, is not completely liquid typically, it has a layered structure imposed by the surfaces, and slips often occur by a layer-over-layer mechanism [162]). The kinetic friction for a liquid lubricant film, even for very thin films (but thicker than two molecular layers), is caused by lubricant viscosity. A lower viscosity implies better lubrication, i.e. lower kinetic friction. Thus, the “best lubricant” is vacuum: the viscosity is zero, so the friction should be zero too (more rigorously, even in the case of a vacuum gap between sliding bodies, due to quantum effects a nonzero friction arises even at zero temperature [190, 191]). Air and water are excellent lubricants (recall how slippery is a thin water film over the ice surface; note also that nature adopted aqueous solutions as a lubricant in the articular joints of animals).

However, a low viscosity easily leads to squeezing out of the lubricant from the sliding interface; then the surfaces come in direct contact and start to be eroded by rubbing wear. That is why in machinery oil-based lubricants are used typically. An oil has large viscosity which leads to high friction, but it is also hard to squeeze out of the contact zone due precisely to its high viscosity. Thus, lubrication engineering is in a permanent search for a compromise: on one hand, the viscosity should be low to provide low friction, but on the other hand, it must be large enough to avoid oil squeezing out and machinery wear. This problem is especially actual for nano-devices, where traditional lubricants often fail to operate.

For a liquid lubricant, the role of the shape of lubricant molecules is also non-trivial. Simulation [192] showed that brush-forming lubricants, e.g. head-glued molecules which work like a hair, provide better lubrication — even if the surfaces

are pushed together so strongly that most lubricant is squeezed out leaving fewer than two monolayers, it continues to operate providing smooth sliding.

To some degree, MD can address relevant realistic features, including the roughness of real surfaces. Even if one polishes the surfaces and makes them smooth, they still consist of domains with different orientation because of the mismatch between the crystalline structures. Simulation [193, 194] showed that when two crystalline surfaces (even with a few lubricant layers in between) are rotated relatively each other, the static friction force changes with the misfit angle over more than one order in magnitude.

Finally, in the case of a lubricant which melts during sliding but solidifies at stick, the formation of solid droplets (grains) pin the surfaces by bridges; but these bridges are not formed instantaneously, not all at once. The bridges, grains, domains, asperities, etc. acquire different sizes and therefore different stress values to be broken at the subsequent slip. The interface is always divided into areas characterized by different thresholds for the onset of sliding. Therefore, such a parameter as the static friction force is in fact not a physical quantity, it describes some average value measured in an experiment (and its value depends on the way the experiment is organized). This fact must be taken into account in description of real tribosystems, and this may be done with the help of the earthquakelike model considered in the next Sec. 5.

5 Earthquakelike Models

An earthquakelike (EQ) model, known also as a multi-contact model, assumes that the contact between two surfaces is realized only at certain points. Typically for a dry contact of rough surfaces these contacts are associated with asperities, but they may otherwise represent molecular bonds or capillary bridges, or they may account for patches of solidified lubricant or its domains for the case of lubricated friction. The contacts are characterized by a continuous distribution of the static threshold values $P_c(x_s)$. A contact itself behaves as follows from MD simulation and tip-based experiments — it operates as an elastic spring until the local shear force $f_i = kx_i$ (k is the elastic constant and x_i is the contact stretchings) is below a threshold value $f_{si} = kx_s$, and breaks when the threshold is exceeded. When the upper block moves, the forces on the contacts increase, and at some moment they start to break in sequence, one after another, with weaker contacts breaking earlier and strongest contacts resisting to the last. Once a contact is broken, it slips and then is reformed again. Such a model was used in many studies [42, 43, 159, 195–200] and successfully accounted for friction at the meso- and macroscale. Models of the same class were also used to describe the failure of fibre bundles and faults [201–203].

The master equation. The EQ model, being the cellular automaton model, allows no analytical treatment. Its kinetics, however, may be reduced to the so-called master equation (ME), also known as the kinetic equation, the Boltzmann equation, etc. It

reads as follows [204, 205]:

$$\left[\frac{\partial}{\partial X} + \frac{\partial}{\partial x} + P(x) \right] Q(x; X) = \delta(x) \int_{-\infty}^{\infty} d\xi P(\xi) Q(\xi; X), \quad (9)$$

where $Q(x; X)$ is the distribution of the stretching x when the bottom of the sliding plate has advanced at position X , and $P(x)\Delta X$ is the fraction of contacts that break at the stretching x when the plate moves by ΔX . The latter is related to the distribution of the breaking thresholds $P_c(x)$ by

$$P(x) = P_c(x)/J_c(x), \quad J_c(x) = \int_x^{\infty} d\xi P_c(\xi), \quad (10)$$

which simply says that the fraction of the contacts that break when X increases by ΔX are those that have their thresholds between x and $x + \Delta X$ divided by the total of fraction $J_c(x)$ of contacts which are not yet broken at stretching x .

(9) and (10) can be generalized to incorporate thermal effects, and can also be supplemented by another equation describing the aging of contacts [205]. The ME can often be solved analytically, thus allowing us to describe the dependence of friction on temperature and velocity, the stick-slip motion and the transition to smooth sliding.

Smooth sliding: friction force versus velocity. The steady-state solution of the ME may be found analytically; it describes the dependence of the kinetic friction force on the sliding velocity in the smooth-sliding regime [206]. According to the second Amontons law (also known as the Coulomb law), the friction force does not depend on the sliding speed; however, this is not true in a general case. The friction force does depend on the speed — $f_k(v)$ increases with v at small velocities, reaches a maximum and then decreases. At low driving velocities the kinetic friction force increases linearly with speed — if the slider moves slowly, all contacts will break sooner or later, purely due to thermal fluctuations. The slower the slider moves, the longer time the contacts have to receive a fluctuation above the threshold, so the smaller is the friction force. The linear $f_k(v)$ dependence sometimes is treated as a (typically very high) “viscosity” of a thin lubricant film [197, 199]. At intermediate speed, the role of thermal fluctuations becomes more and more marginal, and friction is dominated by the so-called aging effects: when a contact breaks, soon it re-forms and grows in size. This leads to a weak (logarithmic) $f_k(v)$ dependence, which is basically consistent with Amontons-Coulomb’s law: the actual $f_k(v)$ dependence is hard to detect experimentally (however, see recent papers [42, 43]). Eventually at high velocities the kinetic friction reaches a maximum and starts to decrease, when sliding is so fast that no time is left for contact re-forming.

Stick-slip: elastic instability. The EQ approach also accounts for the stick-slip motion and the transition to smooth sliding [197, 199, 205]. Roughly speaking, it may be explained as follows: when the slider begins to move, the contacts start to break but they are formed again later. The main question is: do the re-formed contacts produce a force capable to compensate the externally applied driving force? If not, an

elastic instability appears, and the slider will slide fast until the pulling spring force decreases enough; then the process repeats itself. This is the stick-slip regime, typical e.g. of creaking doors and squeaking brakes. If, on the other hand, the reformed contacts build up a force strong enough to compensate the driving one, the system proceeds with smooth sliding. When the aging of contacts is taken into account, such an approach explains the transition from stick-slip to smooth sliding with the increase of driving velocity.

Interaction between the contacts. Above we considered the model with a rigid slider where the contacts do not interact. In reality, elasticity of the sliders leads to contact-contact interaction — when one of contacts breaks, the forces on surrounding contacts should increase by some δf . Numerics [207] shows that $\delta f(r)$ decays with the distance r from the broken contact as $\delta f(r) \propto r^{-1}$ at short distances $r \ll \lambda$, and as $\delta f(r) \propto r^{-3}$ at long distances, where $\lambda \sim a^2 E/k$ is the elastic correlation length [207, 208] expressed in terms of the slider Young modulus E and the average distance a between the contacts. The model may then be simplified by considering the slider as rigid over distances $r \lesssim \lambda$, and treating the contacts within each λ -area as one effective λ -contact with the parameters determined by a corresponding solution of the ME. Numerics also shows that most of the intercontact extra force arises in front and behind the broken contact, which means that the interface may be approximately considered as an effective 1D chain of λ -contacts.

Self-healing crack as a solitary wave. If the λ -contacts do not undergo elastic instability, then a local perturbation spreads smoothly over the interface. Otherwise, if it is subject to the elastic instability, i.e. if it breaks and slides at a certain threshold stress, then the nearest neighboring λ -contacts have a good chance to break too, and a sequence of breaks will propagate through the interface like in a domino effect. In the latter case the dynamics of the chain of λ -contacts can be addressed with the help of the FK model (see Sec. 3), where the sinusoidal substrate potential is replaced by a sawtooth-like potential of periodically repeated inclined pieces [209]. With this approach one can find analytically the maximum and minimum shear stress for crack propagation (the latter corresponds to the Griffith threshold) as well as the crack velocity as function of the applied stress. When the shear stress is uniform and a λ -contact breaks somewhere along the chain, two self-healing cracks propagate from the initial break point in opposite directions as solitary waves similarly to the kink-antikink pair of Fig. 3 until they reach the boundary or meet with another crack created somewhere else.

Onset of sliding. When an elastic slider is pushed from its trailing edge as in the experiments by Fineberg *et al.* [210–212], the nonuniform shear stress is maximal at the trailing edge and falls off with distance inside the block. As the pushing force is increased, the most likely starting event is the breaking of the leftmost λ -contact. Due to interaction between the contacts, this will result in the increase of the stress on the second λ -contact which will break too, and so on until the self-consistent stress will occur below the threshold. Thus, the self-healing crack created at the trailing edge, propagates through the interface over some distance Λ (which can be

found analytically [213]), removing the stress at its tail but creating an extra stress in the region ahead. With a further increase of the pushing force, a second crack is created at the trailing edge. This second crack triggers the previously formed stressed state and propagates further to some distance, and so on until the cracks will reach the leading edge of the system. Besides, when the crack stops, the stress on the contact at crack's tip is close to the threshold value. When the trailing edge moves, the increasing stress is transferred through the interface and affects the contacts ahead of the arrested crack to break one by one. Therefore, between the propagation of fast cracks, the system exhibits a slow dynamics — a creep-like crack motion which may correspond to the slow crack mode observed experimentally [213]. The most important issue here is that, when the cracks propagate through the interface, the whole slider undergoes slight slips, the so-called precursors, which may be detected and used to predict the large earthquake [198, 213]. Recent fully 3D analysis of this class of experiments suggests that precursory activity is an intrinsically quasi-static physical process [214].

Real earthquakes. The EQ-like model described above has been invented initially by Burridge and Knopoff [215] (the famous BK spring-and-block model) to explain real earthquakes, not friction. The physics of these two problems — friction and earthquakes — is essentially similar and differs mainly by the spatio-temporal scale: nanometers and seconds to hours in tribology in comparison to kilometers and years to centuries in geology. Real earthquakes are characterized by two laws — the Gutenberg-Richter (GR) law [216, 217] and the Omori law [218]. Both these laws are empirical, found through long-term statistical observations, and there are no more or less articulate explanations of these laws yet. EQ-like models discussed above may be one of the approaches which would allow to explain both laws. In particular, the GR law may be explained as emerging due to contact aging [219], while the Omori law may be associated with a finite distance of crack propagation — after a large earthquake, not all the stress is released, but a part of it is stored at a distance Λ from the main shock. The eventual goal of these studies is to be able to predict earthquakes, but this has not been achieved yet.

6 Conclusions

Among provisional conclusions of this chapter we mention:

- (i) All levels of modeling and simulation can be highly informative and predictive, provided that specific limitations are kept clear.
- (ii) The simple PT and FK models are extremely useful in understanding several aspects of nanofriction, including superlubricity.
- (iii) MD simulations are powerful and informative for qualitative and even quantitative descriptions of atomic stick-slip and high-speed smooth sliding. An advantage of MD is also that it can address extreme or otherwise unusual frictional situations, still unexplored experimentally [134, 220–222]. The main open problem in

MD is the size and time limitations, in particular the complete omission of slow, logarithmic relaxations and ageing.

(iv) Earthquakelike (multi-contact) models are instrumental in describing mesoscopic friction and fracture, especially in bridging the gap between nano- and macro-scale friction [223].

Among open problems we mention prospective mechanisms for the control of friction. One approach involves using natural or artificially-induced oscillations obtained by small normal or lateral mechanical vibrations which may, when applied at suitable frequency and amplitude ranges, help dislodge a contact, increasing surface mobility and diffusion and thus reducing friction and wear. Flexibility and accessibility are the main relevant features of this approach, since frictional properties can be tuned continuously by the frequency and the amplitude of the applied vibrations. This effect has been demonstrated experimentally with AFM [30, 50, 51, 224] and in sheared confined system [225–227] as well as numerically with MM [48, 49, 228, 229] approaches and with atomistic MD [230, 231]. Despite these promising numerical and experimental contributions, a realistic multi-contact analysis accounting for the friction dependence on vibrations is still to some extent lacking.

Another idea to control friction is to employ a substrate undergoing a phase transition. While it is obvious that friction will change in the presence of a phase transition, it is more subtle to qualify and quantify precisely the effect. Surprisingly perhaps for such a basic concept, there are essentially no experimental data available — and no theory either. A PT-like MD nanofrictional simulation based on a point slider over a 2D model substrate with a built-in structural displacive transition recently predicted that stick-slip friction should actually peak near the substrate critical temperature [232].

Another interesting and practically important topic is AFM manipulation of surface-deposited clusters, which can serve as a useful method to measure the interfacial friction of structurally well-defined contacts of arbitrary size and material combinations. Indeed, one of the remarkable experimental observations of the last decade concerns the unexpected ability of relatively large metal clusters to execute friction-free motions and even long skids with size and shape conservation [233–237]. Gold clusters, comprising typically hundreds of atoms, have been repeatedly observed to diffuse on highly oriented pyrolytic graphite (HOPG) surfaces with surprisingly large thermally activated diffusion coefficients already at room temperature; a similar behavior was reported also for larger antimony clusters. Here, MD simulations are extremely useful in understanding depinning, diffusion, and frictional mechanisms of clusters on surfaces. MD simulations of the diffusive regime have shown the possible coexistence of sticking periods and of long jumps, reminiscent of so-called Levy flights [134, 238–240]. The sticking lasts so long as the cluster-substrate surfaces are orientationally aligned, and the long sliding jumps occur when a thermal fluctuation rotates the cluster destroying the alignment [134].

It is worth mentioning in closing that there remain fully open problems at the very basic theoretical level: we still do not have a proper theory of friction, namely a theory where the frictional work could be calculated quantitatively (not just simulated)

in all cases — they are the majority — where linear-response theory is inapplicable. There are also many more outstanding challenges left in nanofriction, such as:

- The ageing of surface contacts at the nano and macroscales.
- Role of wear and adhesion at the nanoscale.
- Role of ball-shaped molecules (C_{60}) as additives to traditional lubricants [241–243].
- Rolling nanofriction: besides the known case of nanotubes: does it exist, and how to distinguish between rolling and sliding?
- Friction in dislocations and in granular systems.
- Water-based lubricants [244, 245].
- Friction in biological systems (motor proteins, cells membranes and pores, etc.).

Lively progress along these and newer lines is to be expected in the near future.

Acknowledgements We gratefully acknowledge helpful discussion and collaboration with A. Benassi, A.R. Bishop, R. Capozza, R. Guerra, B. Persson, M. Peyrard, G.E. Santoro, J. Scheibert, E. Tosatti, and M. Urbakh. This work is partly funded by the the Italian Ministry of University and Research, the Swiss National Science Foundation Sinergia CRSII2_136287, and the ERC Advanced Grant No. 320796-MODPHYSFRICT. O.B. acknowledges partial support from the EGIDE/Dnipro grant No. 28225UH and from the NASU “RESURS” program.

References

1. M. Urbakh, J. Klafter, D. Gourdon and J. Israelachvili, *Nature (London)* **430**, 525 (2004)
2. V. Bormuth, V. Varga, J. Howard, and E. Schäffer, *Science* **325**, 870 (2009)
3. C. H. Scholz, *Nature (London)* **391**, 37 (1998)
4. F. P. Bowden and D. Tabor, *The Friction and Lubrication of Solids* (Oxford Univ. Press, New York, 1950)
5. R. W. Carpick and M. Salmeron, *Chem. Rev.* **97**, 1163 (1997)
6. G. Binnig, C. F. Quate, and Ch. Gerber, *Phys. Rev. Lett.* **56**, 930 (1986)
7. J. N. Israelachvili, *Surf. Sci. Rep.* **14**, 109 (1992)
8. J. Krim and A. Widom, *Phys. Rev. B* **38**, 12184 (1988)
9. J. Krim, *Sci. Am.* **275**, 74 (1996)
10. A. Vanossi, N. Manini, M. Urbakh, S. Zapperi, and E. Tosatti, *Rev. Mod. Phys.* **85**, 529 (2013)
11. B. N. J. Persson, *Sliding Friction, Physical Properties and Applications* (Springer, Berlin, 2000)
12. C. Mathew Mate, *Tribology on the Small Scale: A Bottom Up Approach to Friction, Lubrication, and Wear (Mesoscopic Physics and Nanotechnology)*, (Oxford Univ. Press, Oxford, 2008)
13. E. Gerde and M. Marder, *Nature (London)* **413**, 285 (2001)
14. C. Marone, *Annu. Rev. Earth Planet. Sci.* **26**, 643 (1998)
15. S. Medyanik, W. K. Liu, In-Ha Sung, and R. W. Carpick, *Phys. Rev. Lett.* **97**, 136106 (2006)
16. L. Prandtl, *Z. Angew. Math. Mech.* **8**, 85 (1928)
17. G. A. Tomlinson, *Philos. Mag.* **7**, 905 (1929)
18. Y. Sang, M. Dubé, and M. Grant, *Phys. Rev. Lett.* **87**, 174301 (2001)
19. O. M. Dudko, A. E. Filippov, J. Klafter and M. Urbakh, *Chem. Phys. Lett.* **352**, 499 (2002)
20. C. E. Maloney and D. J. Lacks, *Phys. Rev. E* **73**, 061106 (2006)

21. J. Kurkijarvi, Phys. Rev. B **6**, 832 (1972)
22. A. Garg, Phys. Rev. B **51**, 15592 (1995)
23. W. L. Johnson and K. A. Samwer, Phys. Rev. Lett. **95**, 195501 (2005)
24. D. J. Lacks, J. Willis, and M. P. Robinson, J. Phys. Chem. B **114**, 10821 (2010)
25. R. Berkovich, S. Garcia-Manyes, M. Urbakh, J. Klafter, and J. M. Fernandez, Biophys. J. **98**, 2692 (2010)
26. J. S. Helman, W. Baltensperger, and J. A. Holyst, Phys. Rev. B **49**, 3831 (1994)
27. R. Gilmore, *Catastrophe Theory for Scientists and Engineers* (Wiley, New York, 1981)
28. A. Socoliuc, R. Bennewitz, E. Gnecco, and E. Meyer, Phys. Rev. Lett. **92**, 134301 (2004)
29. E. Gnecco, R. Bennewitz, T. Gyalog, Ch. Loppacher, M. Bammerlin, E. Meyer, and H.-J. Güntherodt, Phys. Rev. Lett. **84**, 1172 (2000)
30. E. Riedo, E. Gnecco, R. Bennewitz, E. Meyer, and H. Brune, Phys. Rev. Lett. **91**, 084502 (2003)
31. P. Reimann and M. Evstigneev, Phys. Rev. Lett. **93**, 230802 (2004)
32. S. Y. Krylov, K. B. Jinesh, H. Valk, M. Dienwiebel and J. W. M. Frenken, Phys. Rev. E **71**, 65101 (2005)
33. M. Müser, Phys. Rev. B **84**, 125419 (2011)
34. O. K. Dudko, A. E. Filippov, J. Klafter, and M. Urbakh, Proc. Natl. Acad. Sci. U. S. A. **100**, 11378 (2003)
35. S. Stills and R. Overney, Phys. Rev. Lett. **91**, 095501 (2003)
36. A. Schirmeisen, L. Jansen, and H. Fuchs, Phys. Rev. B **71**, 245403 (2005)
37. Q. Li, Y. Dong, D. Perez, A. Martini, and R. W. Carpick, Phys. Rev. Lett. **106**, 126101 (2011)
38. P. Steiner, R. Roth, E. Gnecco, A. Baratoff, S. Maier, T. Glatzel, and E. Meyer, Phys. Rev. B **79**, 045414 (2009)
39. I. Szlufarska, M. Chandross, and R. W. Carpick, J. Phys. D **41**, 123001 (2008)
40. A. Schirmeisen, L. Jansen, H. Holscher, and H. Fuchs, Appl. Phys. Lett. **88**, 123108 (2006)
41. X. Zhao, S. R. Phillpot, W. G. Sawyer, S. B. Sinnott, and S. S. Perry, Phys. Rev. Lett. **102**, 186102 (2009)
42. I. Barel, M. Urbakh, L. Jansen, and A. Schirmeisen, Phys. Rev. Lett. **104**, 066104 (2010)
43. I. Barel, M. Urbakh, L. Jansen, and A. Schirmeisen, Trib. Lett. **39**, 311 (2010)
44. T. Gyalog, M. Bammerlin, R. Lüthi, E. Meyer and H. Thomas, Europhys. Lett. **31**, 269 (1995)
45. R. Prioli, A. F. M. Rivas, F. L. Freire Jr., and A. O. Caride, Appl. Phys. A: Mater. Sci. Process. **76**, 565 (2003)
46. C. Fusco and A. Fasolino, Appl. Phys. Lett. **84**, 699 (2004)
47. C. Fusco and A. Fasolino, Phys. Rev. B **71**, 045413 (2005)
48. M. G. Rozman, M. Urbakh, and J. Klafter, Phys. Rev. E **57**, 7340 (1998)
49. V. Zaloj, M. Urbakh, and J. Klafter, Phys. Rev. Lett. **82**, 4823 (1999)
50. A. Socoliuc, E. Gnecco, S. Maier, O. Pfeiffer, A. Baratoff, R. Bennewitz, and E. Meyer, Science **313**, 207 (2006)
51. M. A. Lantz, D. Wiesmann and B. Gotsmann, Nature Nanotech. **4**, 586 (2009)
52. S. Y. Krylov, J. A. Dijksman, W. A. van Loo, and J. W. M. Frenken, Phys. Rev. Lett. **97**, 166103 (2006)
53. Z. Tshiprut, A. E. Filippov, and M. Urbakh, J. Phys.: Condens. Matter **20**, 354002 (2008)
54. O. M. Braun and Yu. S. Kivshar, *The Frenkel-Kontorova Model: Concepts, Methods, and Applications* (Springer, Berlin, 2004)
55. U. Dehlinger, Ann. Phys. (Leipzig) **2**, 749 (1929)
56. Ya. I Frenkel and T. A. Kontorova, Phys. Z. Sowietunion **13**, 1 (1938)
57. T. A. Kontorova and Ya. I. Frenkel, Zh. Eksp. Teor. Fiz. **8**, 89 (1938)
58. T. A. Kontorova and Ya. I. Frenkel, Zh. Eksp. Teor. Fiz. **8**, 1340 (1938)
59. O. M. Braun, A. R. Bishop, and J. Röder, Phys. Rev. Lett. **79**, 3692 (1997)
60. A. Vanossi, J. Röder, A. R. Bishop, and V. Bortolani, Phys. Rev. E **67**, 016605 (2003)
61. O. M. Braun, Surf. Sci. **230**, 262 (1990)
62. J. D. Meiss, Rev. Mod. Phys. **64**, 795 (1992)
63. S. C. Ying, Phys. Rev. B **3**, 4160 (1971)
64. J. B. Sokoloff, Phys. Rev. B **16**, 3367 (1977)

65. V. L. Pokrovsky and A. L. Talapov, *Zh. Exp. Teor. Fiz.* **75**, 1151 (1978)
66. S. Aubry, in *Solitons and Condensed Matter Physics*, edited by A. R. Bishop and T. Schneider, Springer Series in Solid State Sciences Vol. 8 (Springer, Berlin, 1978), p. 264-277
67. S. Aubry and P. Y. Le Daeron, *Physica D* **8**, 381 (1983)
68. M. Peyrard and S. Aubry, *J. Phys. C: Solid State Phys.* **16**, 1593 (1983)
69. L. M. Floría and J. J. Mazo, *Adv. Phys.* **45**, 505 (1996)
70. Y. Braiman, J. Baumgarten, Joshua Jortner, and J. Klafter, *Phys. Rev. Lett.* **65**, 2398 (1990)
71. A. Benassi, A. Vanossi, and E. Tosatti, *Nature Commun.* **2**, 236 (2011)
72. T. Pruttivarasin, M. Ramm, I. Talukdar, and H. Haeflner, *New J. Phys.* **13**, 075012 (2011)
73. B. Lin and B. Hu, *J. Stat. Phys.* **69**, 1047 (1992)
74. R. S. MacKay, *Renormalization in Area-Preserving Maps* (World Scientific, Singapore, 1993)
75. S. N. Coppersmith and D. S. Fisher, *Phys. Rev. B* **28**, 2566 (1983)
76. S. R. Sharma, B. Bergersen, and B. Joos, *Phys. Rev. B* **29**, 6335 (1984)
77. L. de Seze and S. Aubry: *J. Phys. C* **17**, 389 (1984)
78. S. Aubry and P. Quémenerais, in *Low Dimensional Electronic Properties of Molybdenum Bronzes and Oxides*, ed by C. Schlenker (Kluwer, Dordrecht, 1984)
79. R. S. MacKay, *Physica D* **50**, 71 (1991)
80. M. Hirano and K. Shinjo, *Phys. Rev. B* **41**, 11837 (1990)
81. Hirano and K. Shinjo, *Surf. Sci.* **283**, 473 (1993)
82. K. Shinjo and M. Hirano, *Surf. Sci.* **283**, 473 (1993)
83. M. Dienwiebel, G. S. Verhoeven, N. Pradeep, J. W. M. Frenken, J. A. Heimberg, and H. W. Zandbergen, *Phys. Rev. Lett.* **92**, 126101 (2004)
84. G. S. Verhoeven, M. Dienwiebel, and J. W. M. Frenken, *Phys. Rev. B* **70**, 165418 (2004)
85. M. Dienwiebel, N. Pradeep, G. S. Verhoeven, H. W. Zandbergen, and J. W. M. Frenken, *Surf. Sci.* **576**, 197 (2005)
86. T. Strunz and F.-J. Elmer, *Phys. Rev. E* **58**, 1601 (1998)
87. T. Strunz and F.-J. Elmer, *Phys. Rev. E* **58**, 1612 (1998)
88. J. E. Hammerberg, B. L. Holian, J. Röder, A. R. Bishop, and S. J. Zhou, *Physica D* **123**, 330 (1998)
89. M. Paliy, M., O. Braun, T. Dauxois, and B. Hu, *Phys. Rev. E* **56**, 4025 (1997)
90. O. M. Braun, T. Dauxois, M. V. Paliy, M. Peyrard, and B. Hu, *Physica D* **123**, 357 (1998)
91. T. Bohlein, J. Mikhael, and C. Bechinger, *Nat. Mater.* **11**, 126 (2012)
92. A. Vanossi, N. Manini, and E. Tosatti, *P. Natl. Acad. Sci. USA* **109**, 16429 (2012)
93. M. Peyrard and M. Remoissenet, *Phys. Rev. B* **26**, 2886 (1982)
94. M. Remoissenet and M. Peyrard, *Phys. Rev. B* **29**, 3153 (1984)
95. A. Vanossi, J. Röder, A. R. Bishop, and V. Bortolani, *Phys. Rev. E* **63**, 017203 (2000)
96. T. S. van Erp, A. Fasolino, O. Radulescu, and T. Janssen, *Phys. Rev. B* **60**, 6522 (1999)
97. D. Cule and T. Hwa, *Phys. Rev. Lett.* **77**, 278 (1996)
98. D. Cule and T. Hwa, *Phys. Rev. B* **57**, 8235 (1998)
99. R. Guerra, A. Vanossi, and M. Ferrario, *Surf. Sci.* **601**, 3676 (2007)
100. A. Vanossi and E. Tosatti, *Nature Mater.* **11**, 97 (2012)
101. T. Bohlein and C. Bechinger, *Phys. Rev. Lett.* **109**, 058301 (2012)
102. J. Röder, J. E. Hammerberg, B. L. Holian, and A. R. Bishop, *Phys. Rev. B* **57**, 2759 (1998)
103. B. N. J. Persson, *Phys. Rev. Lett.* **71**, 1212 (1993)
104. B. N. J. Persson, *Phys. Rev. B* **48**, 18140 (1993)
105. B. N. J. Persson, *J. Chem. Phys.* **103**, 3849 (1993)
106. B. N. J. Persson, *Phys. Rev. B* **50**, 4771 (1994)
107. R. P. Mikulla, J. E. Hammerberg, P. S. Lomdahl, and B. L. Holian, *Mat. Res. Soc. Symp. Proc.* **522**, 385 (1998)
108. O. M. Braun, M. V. Paliy, J. Röder, and A. R. Bishop, *Phys. Rev. E* **63**, 036129 (2001)
109. S. Maier, E. Gnecco, A. Baratoff, R. Bennowitz, and E. Meyer, *Phys. Rev. B* **78**, 045432 (2008)
110. M. Gauthier and M. Tsukada, *Phys. Rev. Lett.* **85**, 5348 (2000)

111. R. Bennewitz, A. S. Foster, L. N. Kantorovich, M. Bammerlin, C. Loppacher, S. Schär, M. Guggisberg, E. Meyer, and A. L. Shluger, *Phys. Rev. B* **62**, 2074 (2000)
112. C. Loppacher, R. Bennewitz, O. Pfeiffer, M. Guggisberg, M. Bammerlin, S. Schär, V. Barwich, A. Baratoff, and E. Meyer, *Phys. Rev. B* **62**, 13674 (2000)
113. P. M. Hoffmann, S. Jeffery, J. B. Pethica, H. Özgür Özer, and A. Oral, *Phys. Rev. Lett.* **87**, 265502 (2001)
114. C. Negri, N. Manini, A. Vanossi, G. E. Santoro, and E. Tosatti, *Phys. Rev. B* **81**, 045417 (2010)
115. M. G. Rozman, M. Urbakh, and J. Klafter, *Phys. Rev. Lett.* **77**, 683 (1996)
116. M. G. Rozman, M. Urbakh, and J. Klafter, *Phys. Rev. E* **54**, 6485 (1996)
117. M. H. Müser, *Phys. Rev. Lett.* **89**, 224301 (2002)
118. M. G. Rozman, M. Urbakh, and J. Klafter, *Europhys. Lett.* **39**, 183 (1997)
119. M. G. Rozman, M. M. Urbakh, J. Klafter, and F.-J. Elmer, *J. Phys. Chem. B* **102**, 7924 (1998)
120. O. M. Braun, A. Vanossi, and E. Tosatti, *Phys. Rev. Lett.* **95**, 026102 (2005)
121. A. Vanossi, N. Manini, G. Divitini, G. E. Santoro, and E. Tosatti, *Phys. Rev. Lett.* **97**, 056101 (2006)
122. G. E. Santoro, A. Vanossi, N. Manini, G. Divitini, and E. Tosatti, *Surf. Sci.* **600**, 2726 (2006)
123. A. Vanossi, N. Manini, F. Caruso, G. E. Santoro, and E. Tosatti, *Phys. Rev. Lett.* **99**, 206101 (2007)
124. N. Manini, M. Cesaratto, G. E. Santoro, E. Tosatti, and A. Vanossi, *J. Phys.: Condens. Matter* **19**, 305016 (2007)
125. R. L. Woulaché, A. Vanossi, and N. Manini, *Phys. Rev. E* **88**, 012810 (2013)
126. I. E. Castelli, N. Manini, R. Capozza, A. Vanossi, G. E. Santoro, and E. Tosatti, *J. Phys.: Condens. Matter* **20**, 354005 (2008)
127. I. E. Castelli, R. Capozza, A. Vanossi, G. E. Santoro, N. Manini, and E. Tosatti, *J. Chem. Phys.* **131**, 174711 (2009)
128. C. Drummond and J. Israelachvili, *Phys. Rev. E* **63**, 041506 (2001)
129. C. Drummond, J. Israelachvili, and P. Richetti, *Phys. Rev. E* **67**, 066110 (2003)
130. M. Weiss and F.-J. Elmer, *Phys. Rev. B* **53**, 7539 (1996)
131. M. Weiss and F.-J. Elmer, *Z. Phys. B* **104**, 55 (1997)
132. M. Igarashi, A. Nator, and J. Nakamura, *Phys. Rev. B* **78**, 165427 (2008)
133. W. K. Kim and M. L. Falk, *Phys. Rev. B* **80**, 235428 (2009)
134. R. Guerra, U. Tartaglino, A. Vanossi, and E. Tosatti, *Nature Mater.* **9**, 634 (2010)
135. M. O. Robbins and M. H. Müser, in *Modern Tribology Handbook*, edited by B. Bhushan (CRC Press, Boca Raton, FL, 2001), p. 717
136. M. H. Müser, *Computer Simulations in Condensed Matter Systems: From Materials to Chemical Biology Vol. 2, Lecture Notes in Physics Vol. 704*, edited by M. Ferrario, G. Ciccotti, and K. Binder (Springer, Heidelberg, 2006), p. 65
137. R. Car and M. Parrinello, *Phys. Rev. Lett.* **55**, 2471 (1985)
138. C. H. Xu, C. Z. Wang, C. T. Chan, and K. M. Ho, *J. Phys.: Condens. Matter* **4**, 6047 (1992)
139. B. J. Garrison and D. Srivastava, *Ann. Rev. Phys. Chem.* **46**, 373 (1995)
140. D. W. Brenner, O. A. Shenderova, and A. Areshkin, *Quantum-Based Analytic Interatomic Forces and Materials Simulation, Reviews in Computational Chemistry*, edited by K. B. Lipkowitz and D. B. Boyd (VCH Publishers, New York, 1998), p. 213
141. S. J. Weiner, P. A. Kollman, D. T. Nguyen, and D. A. Case, *J. Comp. Chem.* **7**, 230 (1986)
142. J. H. Los, L. M. Ghiringhelli, E. J. Meijer, and A. Fasolino, *Phys. Rev. B* **72**, 214102 (2005)
143. L. M. Ghiringhelli, J. H. Los, A. Fasolino, and E. J. Meijer, *Phys. Rev. B* **72**, 214103 (2005)
144. S. J. Stuart, *J. Chem. Phys.* **112**, 6472 (2000)
145. D. W. Brenner, O. A. Shenderova, J. A. Harrison, S. J. Stuart, B. Ni, and S. B. Sinnott, *J. Phys.: Condens. Matter* **14**, 783 (2002)
146. A. C. T. van Duin, S. Dasgupta, F. Lorant, and W. A. Goddard III, *J. Phys. Chem. A* **105**, 9396 (2001)
147. M. S. Tomassone, J. B. Sokoloff, A. Widom, and J. Krim, *Phys. Rev. Lett.* **79**, 4798 (1997)
148. O. M. Braun and M. Peyrard, *Phys. Rev. E* **63**, 046110 (2001)

149. O. M. Braun and R. Ferrando, *Phys. Rev. E* **65**, 061107 (2002)
150. V. B. Magalinskii, *Sov. Phys. JETP* **9**, 1381 (1959)
151. R. J. Rubin, *J. Math. Phys.* **1**, 309 (1960)
152. R. Zwanzig, *J. Stat. Phys.* **9**, 215 (1973)
153. X. Li and W. E, *Phys. Rev. B* **76**, 104107 (2007)
154. L. Kantorovich, *Phys. Rev. B* **78**, 094304 (2008)
155. L. Kantorovich and N. Rompotis, *Phys. Rev. B* **78**, 094305 (2008)
156. A. Benassi, A. Vanossi, G. E. Santoro, and E. Tosatti, *Phys. Rev. B* **82**, 081401 (2010)
157. A. Benassi, A. Vanossi, G. E. Santoro, and E. Tosatti, *Tribol. Lett.* **48**, 41 (2012)
158. O. M. Braun, N. Manini, and E. Tosatti, *Phys. Rev. Lett.* **110**, 085503 (2013)
159. O. M. Braun and J. Röder, *Phys. Rev. Lett.* **88**, 096102 (2002)
160. B. Luan and M. O. Robbins, *Phys. Rev. Lett.* **93**, 036105 (2004)
161. O. M. Braun, M. Peyrard, V. Bortolani, A. Franchini, and A. Vanossi, *Phys. Rev. E* **72**, 056116 (2005)
162. O. M. Braun and A. G. Naumovets, *Surf. Sci. Rep.* **60**, 79 (2006)
163. A. F. Voter, F. Montalenti, and T. C. Germann, *Annu. Rev. Mater. Res.* **32**, 321 (2002)
164. Y. Mishin, A. Suzuki, B. P. Uberuaga, and A. F. Voter, *Phys. Rev. B* **75**, 224101 (2007)
165. W. K. Kim and M. L. Falk, *Phys. Rev. B* **84**, 165422 (2011)
166. J. H. Dieterich and B. D. Kilgore, *Pure Appl. Geophys.* **143**, 283 (1994)
167. A. Ruina, *J. Geophys. Res.* **88**, 10359 (1983)
168. F. Heslot, T. Baumberger, B. Perrin, B. Caroli, and C. Caroli, *Phys. Rev. E* **49**, 4973 (1994)
169. Q. Li, T. E. Tullis, D. Goldsby, and R. W. Carpick, *Nature* **480**, 233 (2011)
170. E. McGee, R. Smith, and S. D. Kenny, *Int. J. Mater. Res.* **98**, 430 (2007)
171. B. Q. Luan, S. Hyun, J. F. Molinari, N. Bernstein, M. O. Robbins, *Phys. Rev. E* **74**, 046710 (2006)
172. W. E, W. Q. Ren, and E. Vanden-Eijnden, *J. Comput. Phys.* **228**, 5437 (2009)
173. A. Z. Szeri, in *Modern Tribology Handbook*, edited by B. Bhushan (CRC Press, Boca Raton, FL, 2001), p. 384
174. H. Yoshizawa and J. Israelachvili, *J. Phys. Chem.* **97**, 11300 (1993)
175. J. Gao, W. D. Luedtke, and U. Landman, *Phys. Rev. Lett.* **79**, 705 (1997)
176. J. Gao, W. D. Luedtke, and U. Landman, *J. Chem. Phys.* **106**, 4309 (1997)
177. B. N. J. Persson and E. Tosatti, *Phys. Rev. B* **50**, 5590 (1994)
178. B. N. J. Persson and F. Mugele, *J. Phys.: Condens. Matter* **16**, R295 (2004)
179. U. Tartaglino, I. M. Sivebaek, B. N. J. Persson, and E. Tosatti, *J. Chem. Phys.* **125**, 014704 (2006)
180. M. J. Stevens and M. O. Robbins, *Phys. Rev. E* **48**, 3778 (1993)
181. P. A. Thompson and M. O. Robbins, *Science* **250**, 792 (1990)
182. O. M. Braun and M. Peyrard, *Phys. Rev. E* **68**, 011506 (2003)
183. A. V. Zhukov, M. V. Paliy, O. M. Braun, and T. F. George, *Phys. Lett. A* **361**, 437 (2007)
184. C. D. Lorenz, M. Chandross, and G. S. Grest, *J. Adhesion Sci. Technol.* **24**, 2453 (2010)
185. C. D. Lorenz, M. Chandross, J. M. D. Lane, and G. S. Grest, *Model. Simul. Mat. Sci. Engin.* **18**, 034005 (2010)
186. M. Chandross, E. B. Webb, M. J. Stevens, G. S. Grest, and S. H. Garofalini, *Phys. Rev. Lett.* **93**, 166103 (2004)
187. M. Chandross, C. D. Lorenz, M. J. Stevens, and G. S. Grest, *Langmuir* **24**, 1240 (2008)
188. M. H. Müser and M. O. Robbins, *Phys. Rev. B* **61**, 2335 (2000)
189. O. M. Braun, M. Paliy, and S. Consta, *Phys. Rev. Lett.* **92**, 256103 (2004)
190. A. I. Volokitin and B. N. J. Persson, *Rev. Mod. Phys.* **79**, 1291 (2007)
191. A. I. Volokitin and B. N. J. Persson, *Phys. Rev. Lett.* **106**, 094502 (2011)
192. O. M. Braun, N. Manini, and E. Tosatti, *Phys. Rev. B* **78**, 195402 (2008)
193. O. M. Braun and N. Manini, *Phys. Rev. E* **83**, 021601 (2011)
194. N. Manini and O. M. Braun, *Phys. Lett. A* **375**, 2946 (2011)
195. B. N. J. Persson, *Phys. Rev. B* **51**, 13568 (1995)
196. A. E. Filippov, J. Klafter, and M. Urbakh, *Phys. Rev. Lett.* **92**, 135503 (2004)
197. O. M. Braun and E. Tosatti, *Europhys. Lett.* **88**, 48003 (2009)

198. O. M. Braun, I. Barel, and M. Urbakh, *Phys. Rev. Lett.* **103**, 194301 (2009)
199. O. M. Braun and E. Tosatti, *Philos. Mag.* **91**, 3253 (2011)
200. R. Capozza and M. Urbakh, *Phys. Rev. B* **86**, 085430 (2012)
201. R. F. Smalley, D. L. Turcotte, and S. A. Solla J. *Geophys. Res.* **90**, 1894 (1985)
202. W. I. Newman and A. M. Gabriellov, *Int. J. Fracture* **50**, 1 (1991)
203. W. I. Newman and S. L. Phoenix, *Phys. Rev. E* **63**, 021507 (2001)
204. O. M. Braun and M. Peyrard, *Phys. Rev. Lett.* **100**, 125501 (2008)
205. O. M. Braun and M. Peyrard, *Phys. Rev. E* **82**, 036117 (2010)
206. O. M. Braun and M. Peyrard, *Phys. Rev. E* **83**, 046129 (2011)
207. O. M. Braun, M. Peyrard, D. V. Stryzheus, and E. Tosatti, *Collective effects at frictional interfaces*, *Tribology Letters* **48**, 11 (2012)
208. C. Caroli and Ph. Nozieres, *Eur. Phys. J. B* **4**, 233 (1998)
209. O. M. Braun and M. Peyrard, *Phys. Rev. E* **85**, 026111 (2012)
210. S. M. Rubinstein, G. Cohen, and J. Fineberg, *Nature (London)* **430**, 1005 (2004)
211. S. M. Rubinstein, G. Cohen, and J. Fineberg, *Phys. Rev. Lett.* **96**, 256103 (2006)
212. S. M. Rubinstein, I. Barel, Z. Reches, O. M. Braun, M. Urbakh, and J. Fineberg, *Pure Appl. Geophys.* **168**, 2151 (2011)
213. O. M. Braun, M. Peyrard, and J. Scheibert, unpublished (2014)
214. A. Taloni, A. Benassi, and S. Zapperi, preprint arXiv:1307.2742 (2013)
215. R. Burridge and L. Knopoff, *Bull. Seismol. Soc. Am.* **57**, 341 (1967)
216. B. Gutenberg and C. F. Richter, *Bull. Seismol. Soc. Am.* **46**, 105 (1954)
217. B. Gutenberg and C. F. Richter, *Ann. Geophys.* **9**, 1 (1956)
218. F. Omori, *J. Coll. Sci. Imp. Univ. Tokyo* **7**, 111 (1894)
219. O. M. Braun and M. Peyrard, *Phys. Rev. E* **87**, 032808 (2013)
220. U. Tartaglino, T. Zykova-Timan, F. Ercolessi, and E. Tosatti, *Phys. Repts.* **411**, 291 (2005)
221. T. Zykova-Timan, D. Ceresoli, U. Tartaglino, and E. Tosatti, *Phys. Rev. Lett.* **94**, 176105 (2005)
222. T. Zykova-Timan, D. Ceresoli, and E. Tosatti, *Nature Mater.* **6**, 231 (2007)
223. O. M. Braun, *Tribol. Lett.* **39**, 283 (2010)
224. S. Jeon, T. Thundat, and Y. Braiman, *Appl. Phys. Lett.* **88**, 214102 (2006)
225. M. Heuberger, C. Drummond, and J. N. Israelachvili, *J. Phys. Chem. B* **102**, 5038 (1998)
226. L. Bureau, T. Baumberger, and C. Caroli, *Phys. Rev. E* **62**, 6810 (2000)
227. A. Cochard, L. Bureau, and T. Baumberger, *Trans. ASME* **70**, 220 (2003)
228. Z. Tshiprut, A. E. Filippov, and M. Urbakh, *Phys. Rev. Lett.* **95**, 016101 (2005)
229. R. Guerra, A. Vanossi, and M. Urbakh, *Phys. Rev. E* **78**, 036110 (2008)
230. J. Gao, W. Luedtke, and U. Landman, *J. Phys. Chem. B* **102**, 5033 (1998)
231. R. Capozza, A. Vanossi, A. Vezzani, and S. Zapperi, *Phys. Rev. Lett.* **103**, 085502 (2009)
232. A. Benassi, A. Vanossi, G. E. Santoro, and E. Tosatti, *Phys. Rev. Lett.* **106**, 256102 (2011)
233. L. Bardotti, P. Jensen, A. Hoareau, M. Treilleux, B. Cabaud, A. Perez, and F. Cadete Santos Aires, *Surf. Sci.* **367**, 276 (1996)
234. J. Brndiar, R. Turanský, D. Dietzel, A. Schirmeisen, and I. Štich, *Nanotechnology* **22**, 085704 (2011)
235. D. Dietzel, C. Ritter, T. Mönninghoff, H. Fuchs, A. Schirmeisen, and U. D. Schwarz, *Phys. Rev. Lett.* **101**, 125505 (2008)
236. G. Paolicelli, K. Mougín, A. Vanossi, and S. Valeri, *J. Phys.: Condens. Matter* **20**, 354011 (2008)
237. G. Paolicelli, M. Rovatti, A. Vanossi, and S. Valeri, *Appl. Phys. Lett.* **95**, 143121 (2009)
238. W. Luedtke and U. Landman, *Phys. Rev. Lett.* **82**, 3835 (1999)
239. L. J. Lewis, P. Jensen, N. Combe, and J-L. Barrat, *Phys. Rev. B* **61**, 16084 (2000)
240. Y. Maruyama, *Phys. Rev. B* **69**, 245408 (2004)
241. O. M. Braun, *Phys. Rev. Lett.* **95**, 126104 (2005)
242. O. M. Braun and E. Tosatti, *J. Phys.: Condens. Matter* **20**, 354007 (2008)
243. O. M. Braun and E. Tosatti, *Phil. Mag. Lett.* **88**, 509 (2008)
244. M. Paliy, O. M. Braun, and S. Consta, *Tribology Letters* **23**, 7 (2006)
245. M. Paliy, O. M. Braun, and S. Consta, *J. Phys. Chem. C* **116**, 8932 (2012)